CHAPTER 8
CHARACTERISATION OF ALKALI FUSION PROCESSES

8.1 INTRODUCTION

De Wet's patent has the advantage of synthesising a stable basic sulphate at a fast rate. The sulphate is so stable such that it can be washed with mineral acids [4], for example HCl, to remove radioactive impurities. The characterisation of the process will now be given. Figure 7.1 shows a diagrammatic representation of the process for zirconia recovery and the methods used for analysis in bold.

The alkali fusion process was followed stepwise with characterisation methods. The characterisation focused on identifying the phases present and quantifying their composition. The by-products and effluents were also investigated using elemental analysis. The final products are further characterised with spectroscopic methods and SEM.

8.2 RESULTS

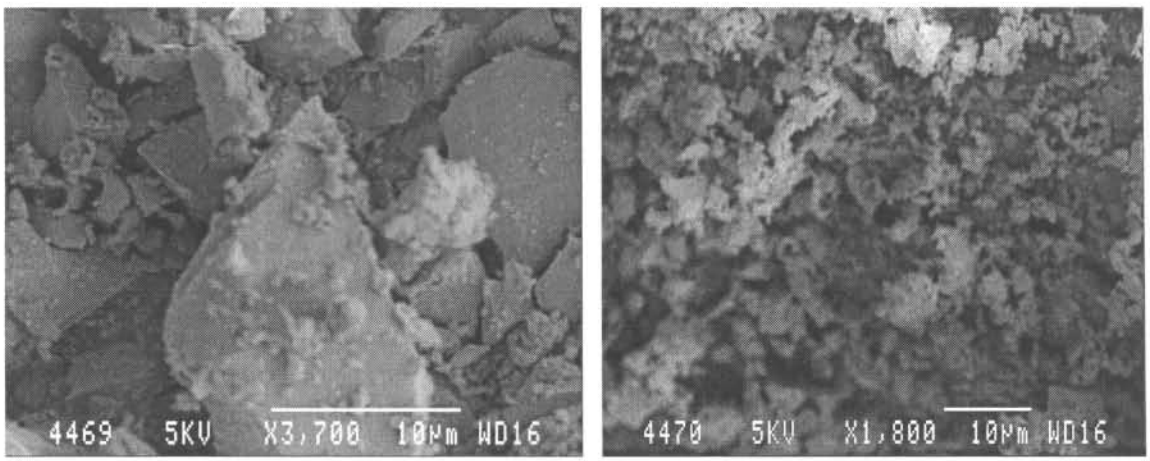

(a) b)

FIGURE 8.1: SEM photographs of milled zircon sand mined at Richards Bay, (a) the 45µm and (b) the 9µm mean particle size. The difference in particle size can be seen.

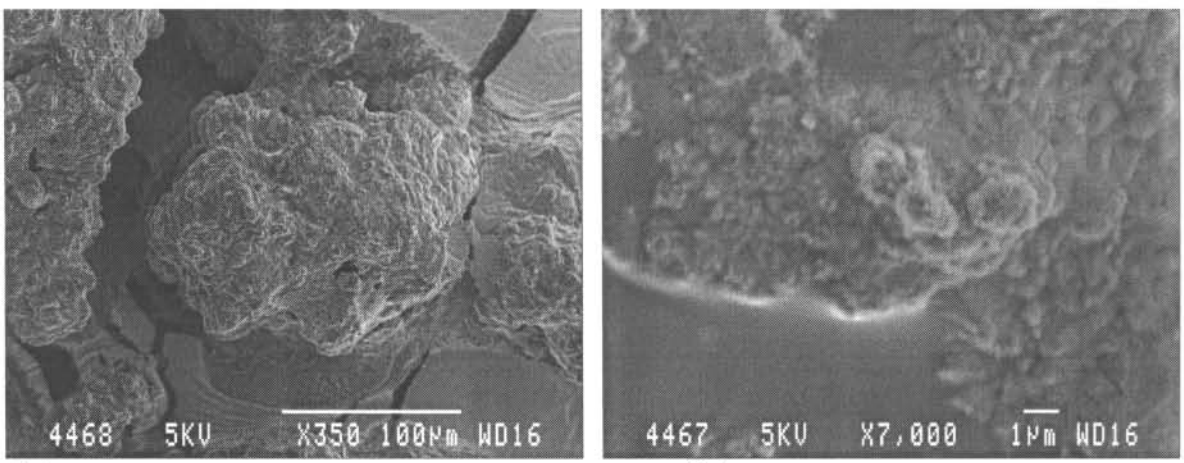

(a) (b)

FIGURE 8.2: SEM photographs of decomposed zircon sand (AFDZ). The AFDZ was obtained by zircon with sodium hydroxide for an hour. The particle size of the agglomerate of the fused product is shown in (a). On the surface of (b), some unreacted NaOH can be seen as the homogenised area. The unreacted NaOH was common for all the fusion without the intermediate milling.

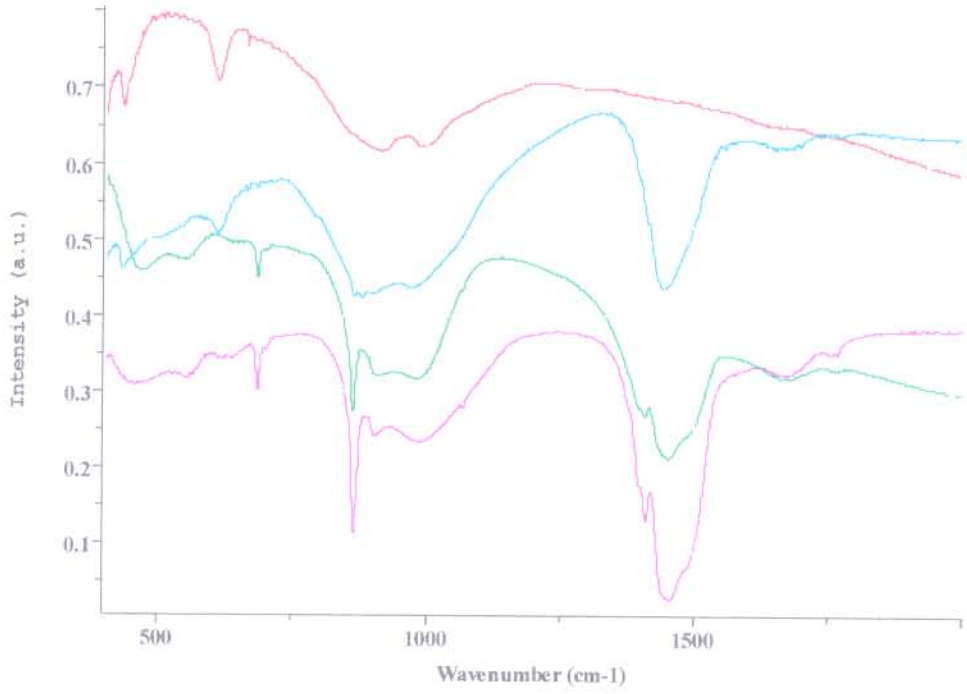

FIGURE 8.3: A super-positioning of the infrared spectra of alkali fused decomposed zircon at 650°C. The spectrum at the top represents milled zircon sand. Following consecutively are the spectra for 2, 4, and 6 moles NaOH fused with a mole of zircon sand for about an hour.

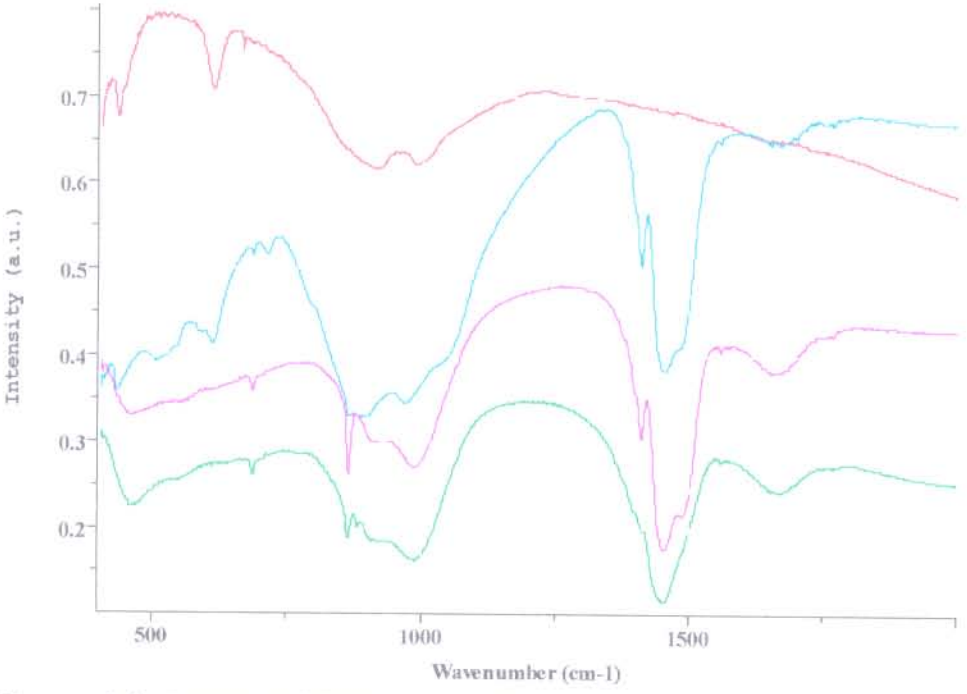

FIGURE 8.4: A super-positioning of the infrared spectra of alkali fused decomposed zircon at 750°C. The spectrum at the top represents milled zircon sand. Following consecutively are the spectra for 2, 4, and 6 moles NaOH fused with a mole of zircon sand for about an hour.

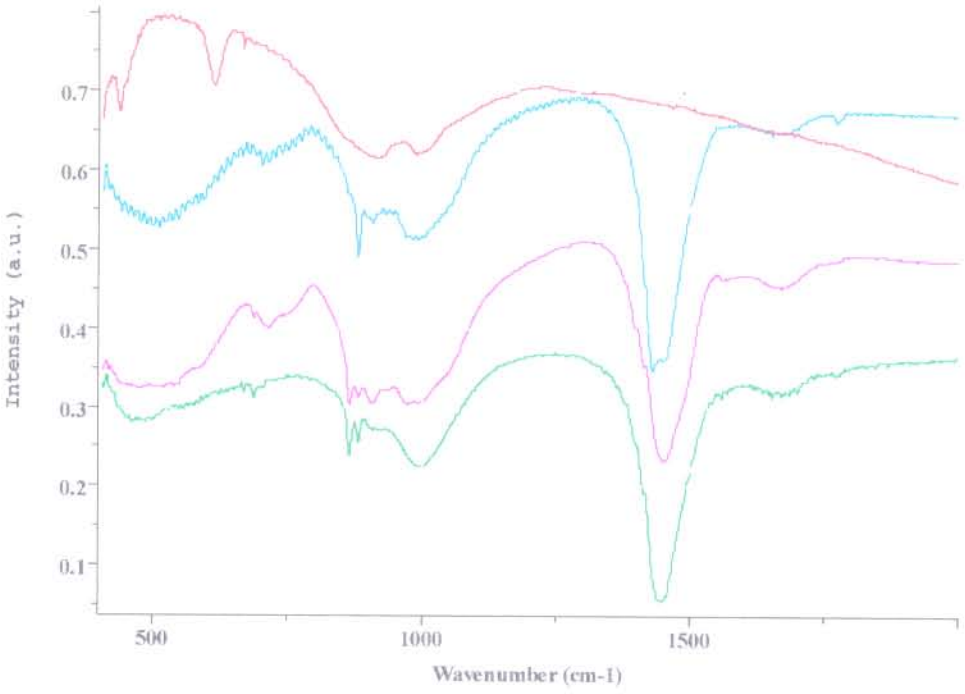

FIGURE 8.5: A super-positioning of the infrared spectra of alkali fused decomposed zircon at 850°C. The spectrum at the top represents milled zircon sand. Following consecutively are the spectra for 2, 4, and 6 moles NaOH fused with a mole of zircon sand for about an hour.

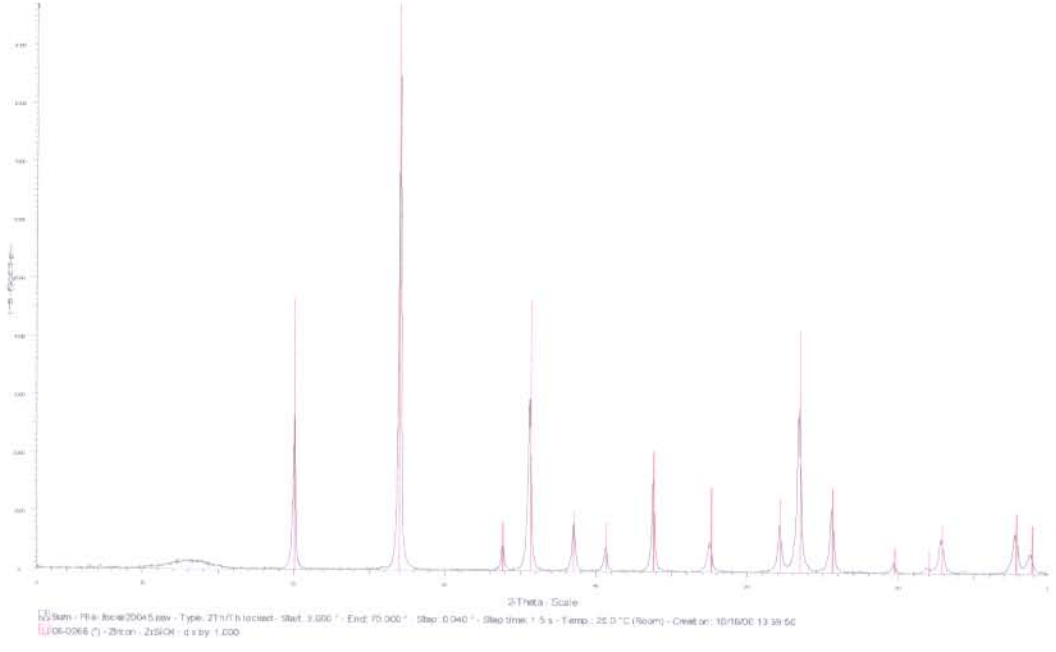

FIGURE 8.6: X-ray spectra of milled zircon sand, $d_{50} \approx 9\mu m$, from Richard's bay.

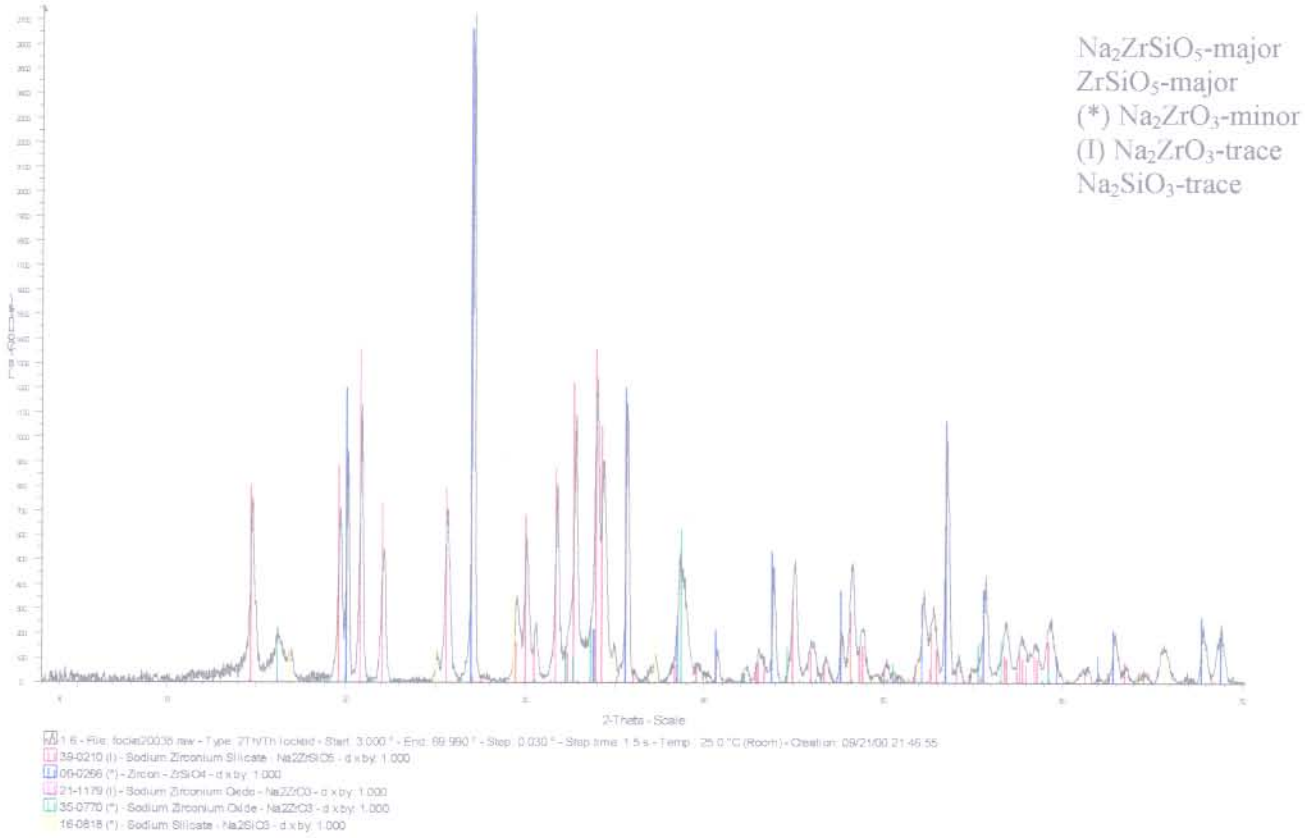

FIGURE 8.7: X-ray diffraction pattern of alkali fused decomposed zircon. A mole of $d_{50} \approx 9\mu m$ zircon was decomposed with two moles of sodium hydroxide at 850°C for about 2 hours with intermediate milling.

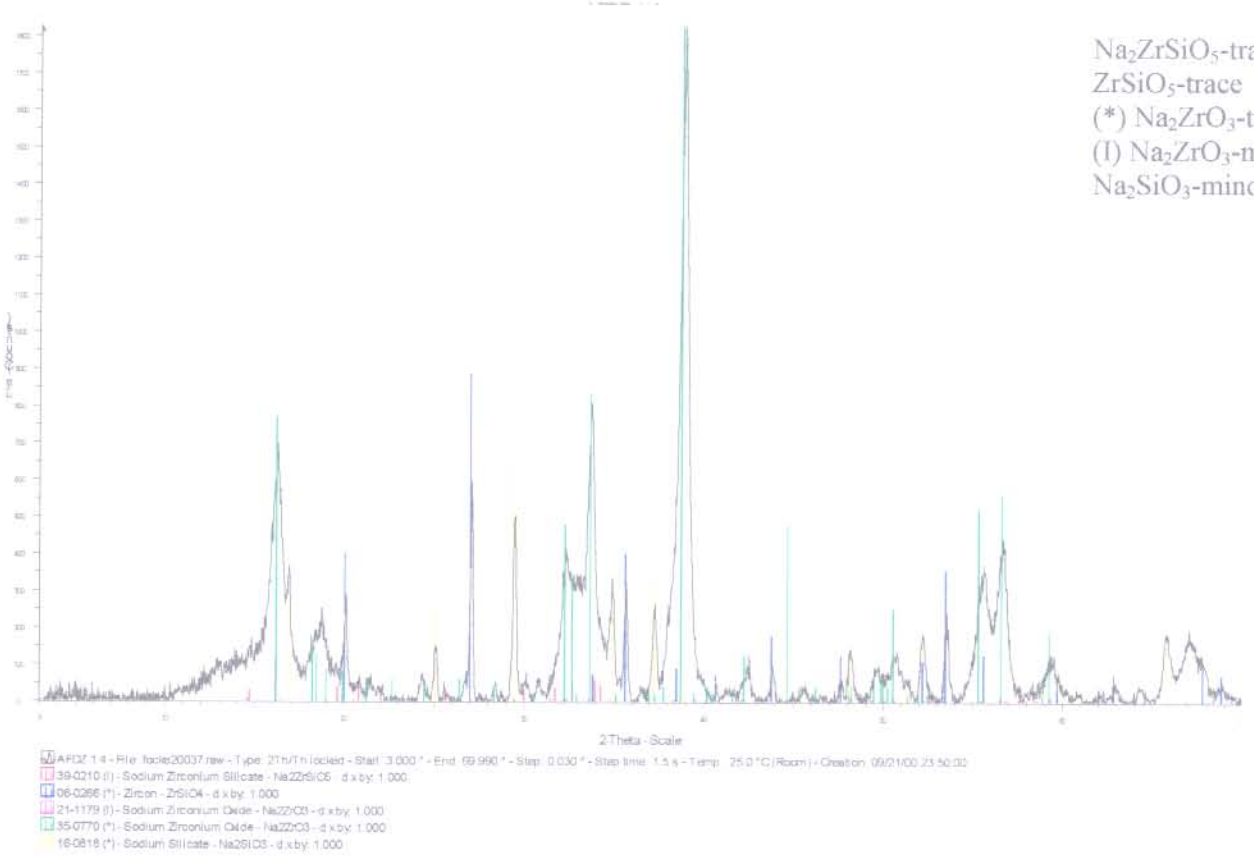

FIGURE 8.8: X-ray diffraction pattern of alkali fused decomposed zircon. A mole of $d_{50} \approx 9\mu m$ zircon was decomposed with four moles of sodium hydroxide at 850°C for 2 hours with intermediate milling.

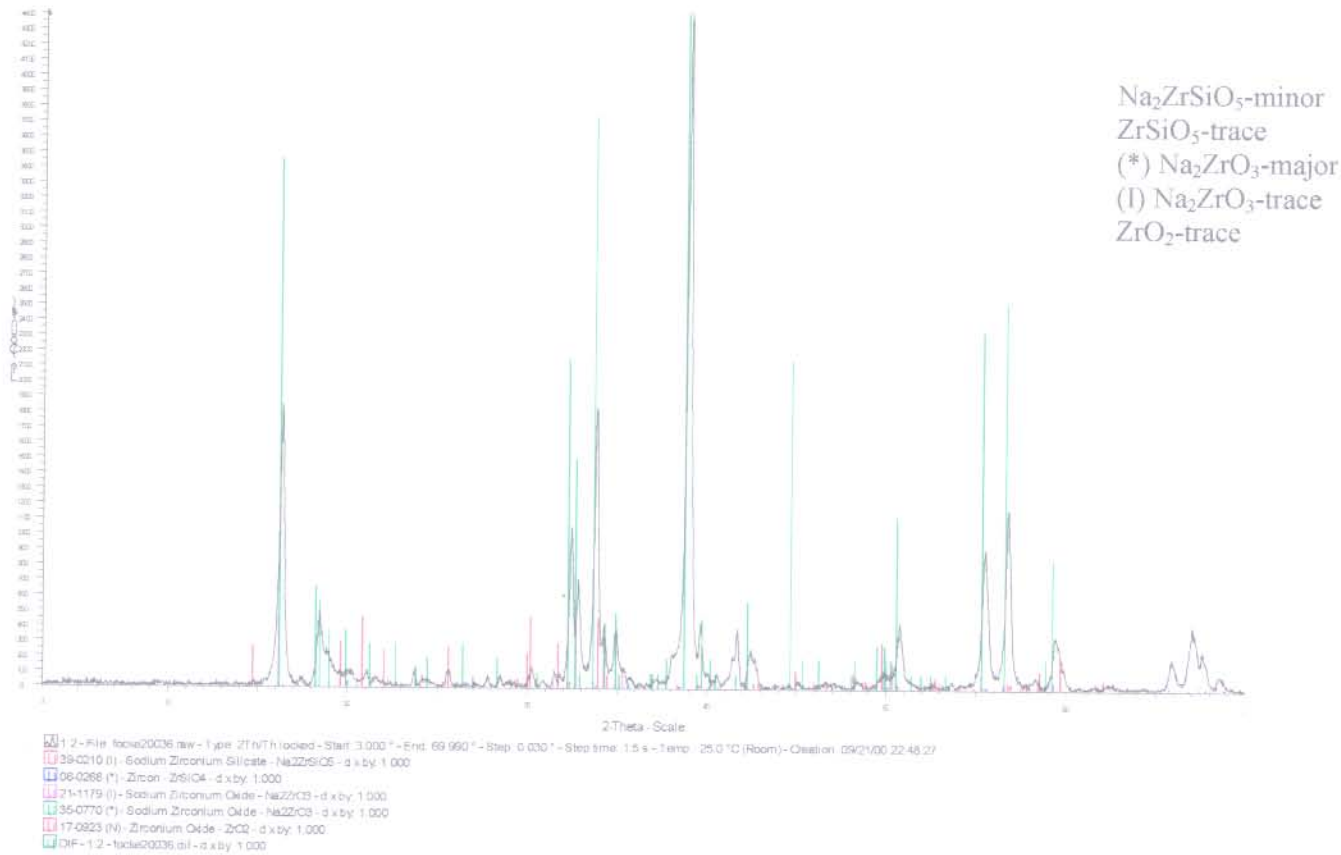

FIGURE 8.9: X-ray diffraction pattern of alkali fused decomposed zircon. A mole of $d_{50} \approx 9\mu m$ zircon was decomposed with six moles of sodium hydroxide at 850°C for 2 hours with intermediate milling.

FIGURE 8.10: A super-positioning of the X-ray diffraction pattern of alkali fused decomposed zircon. The spectra at for the various mole ratios at 850°C were superimposed. At the top is the spectra when fusing with six moles of NaOH. Following consecutively is the spectra when fusing with four and two moles of NaOH.

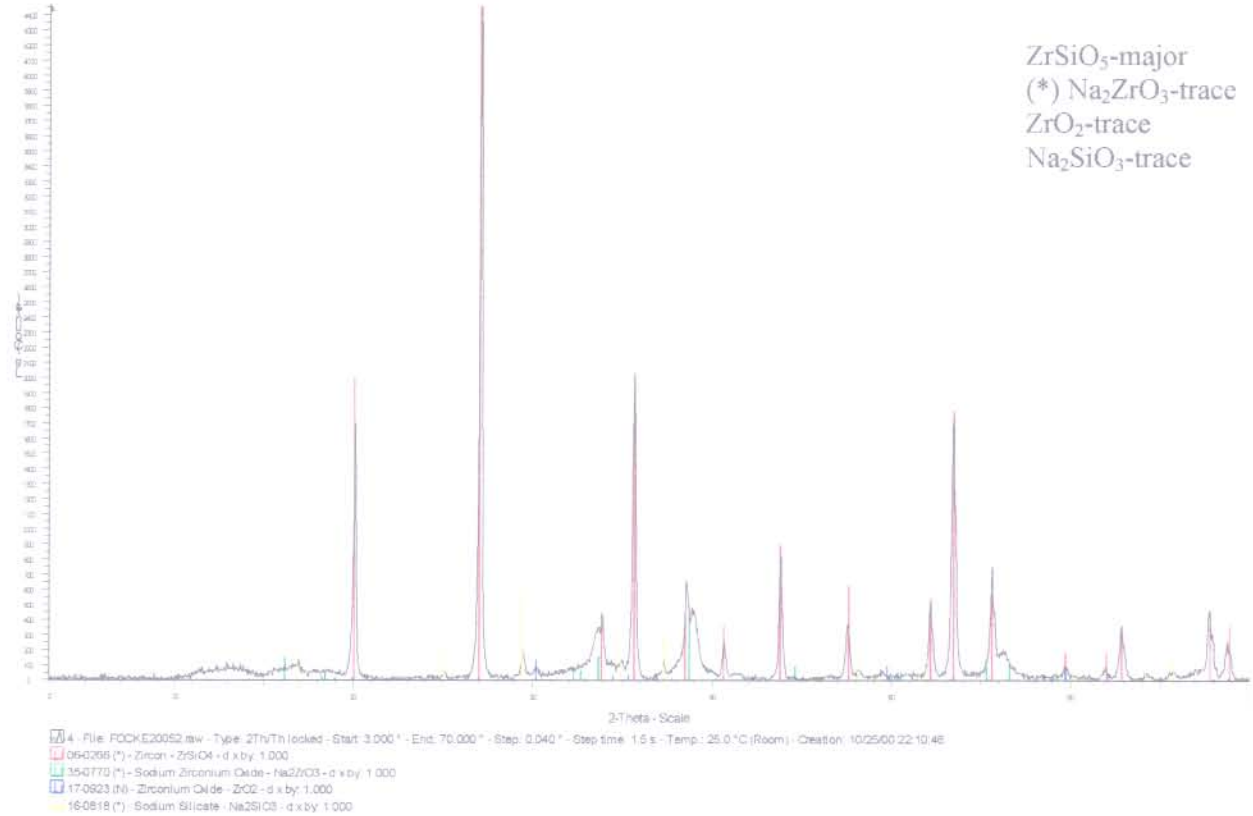

FIGURE 8.11: X-ray diffraction pattern of alkali fused decomposed zircon. A mole of $d_{50} \approx 9\mu m$ zircon was decomposed with two moles of sodium hydroxide at 650°C for 2 hours with intermediate milling.

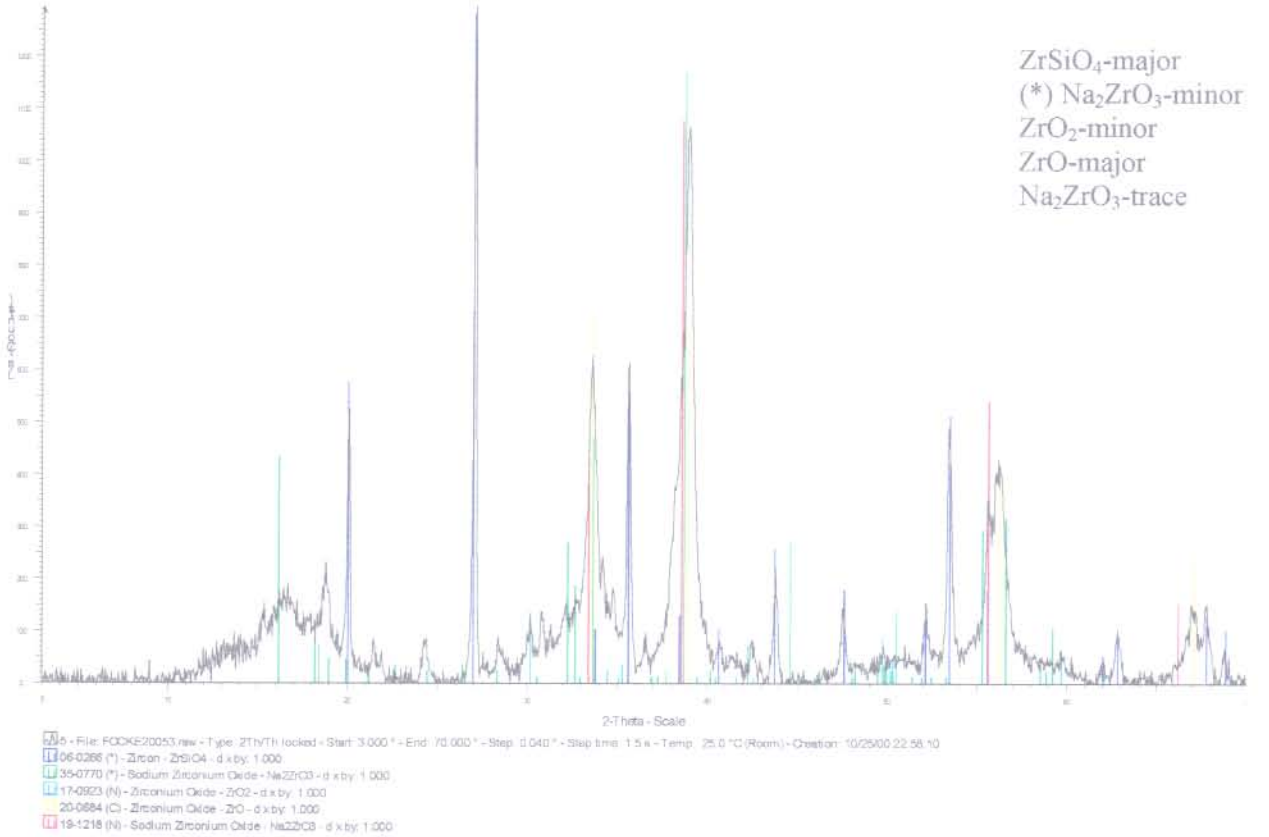

FIGURE 8.12: X-ray diffraction pattern of alkali fused decomposed zircon. A mole of $d_{50} \approx 9\mu m$ zircon was decomposed with four moles of sodium hydroxide at 650°C for 2 hours with intermediate milling.

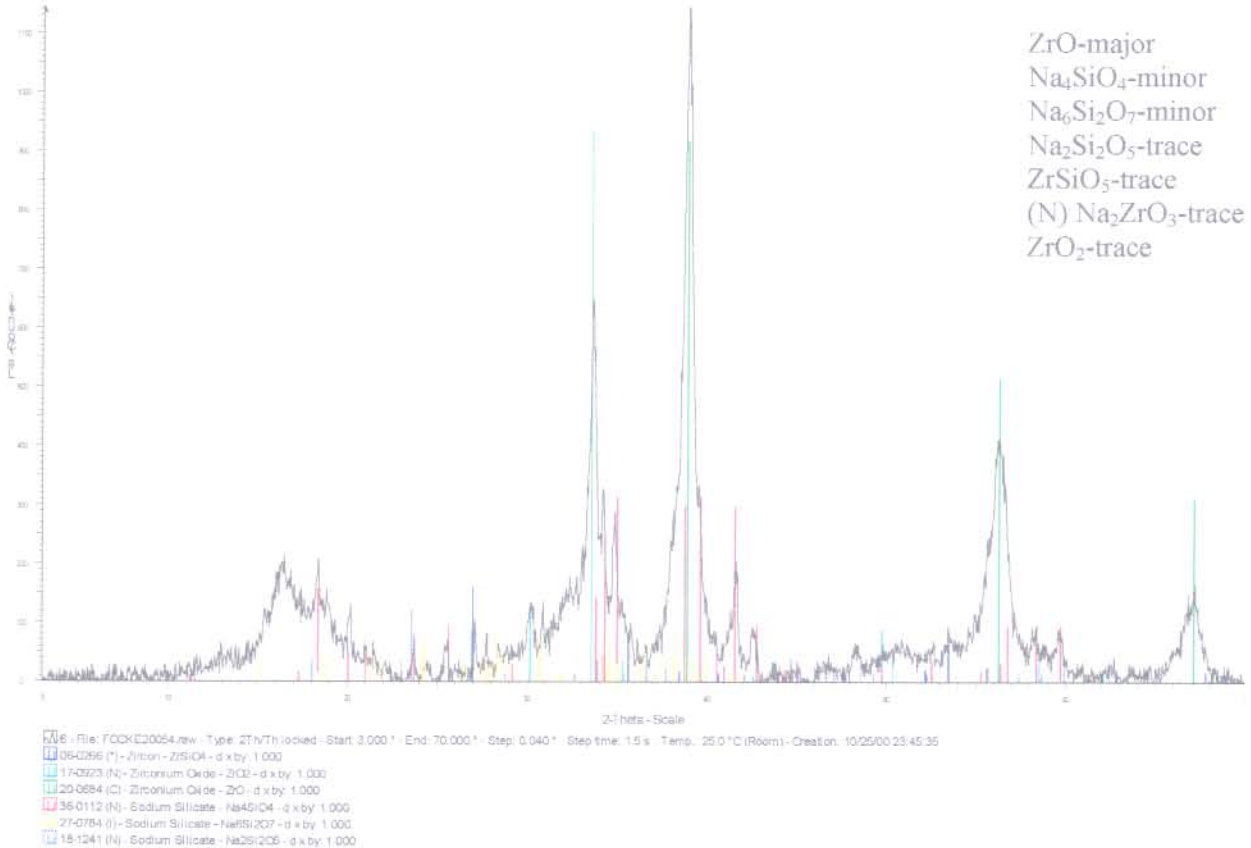

FIGURE 8.13: X-ray diffraction pattern of alkali fused decomposed zircon. A mole of $d_{50} \approx 9\mu m$ zircon was decomposed with six moles of sodium hydroxide at 650°C for 2 hours with intermediate milling.

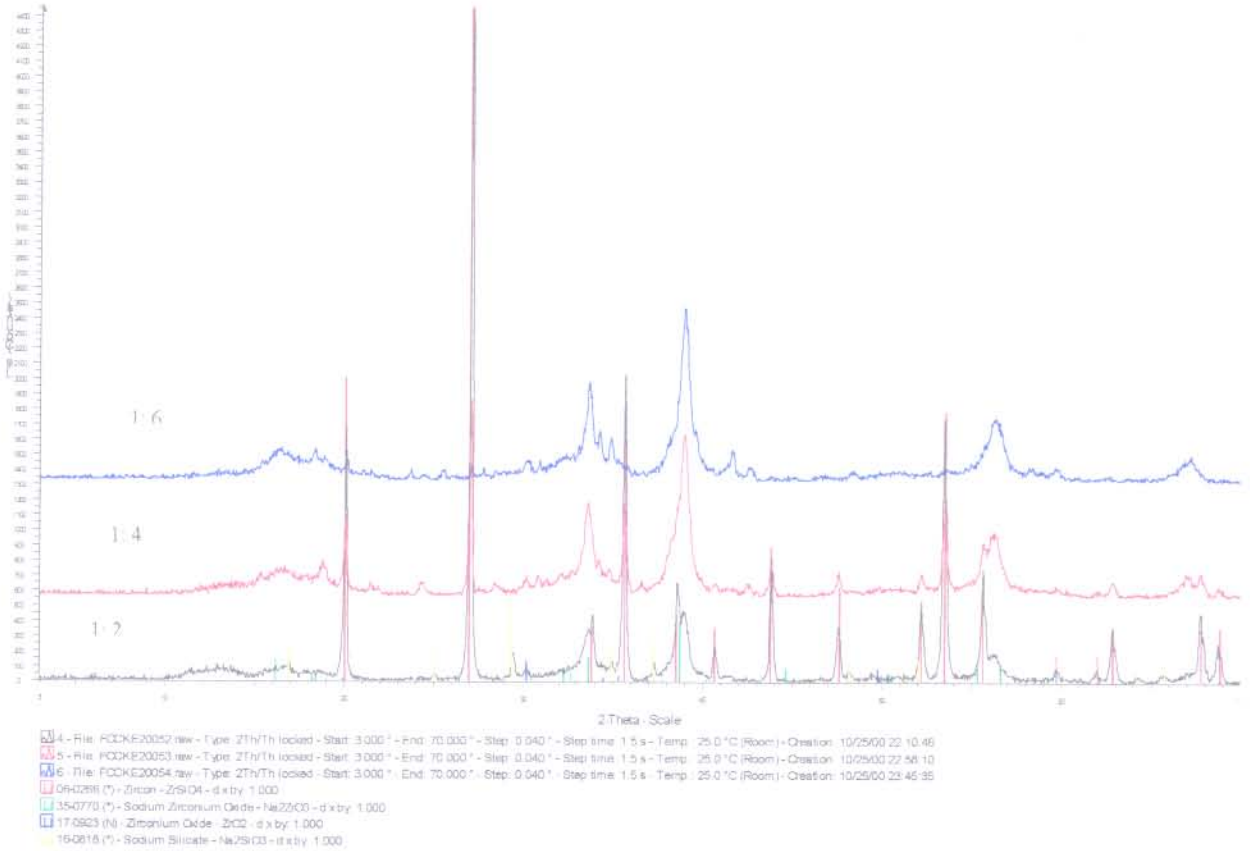

FIGURE 8.14: A super-positioning of the X-ray diffraction pattern of alkali fused decomposed zircon. The spectra at for the various mole ratios at 650°C after two hours with intermediate milling were superimposed.

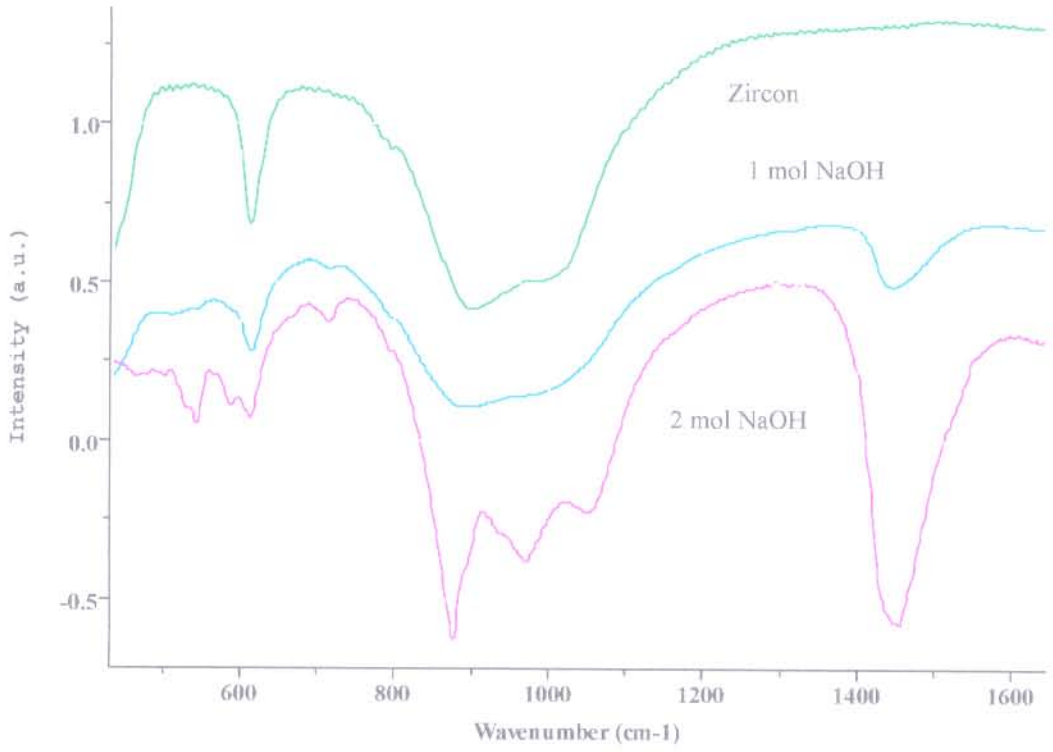

Figure 8.15: A super-positioning of the Infra red spectra of alkali fused decomposed zircon. The spectra at for the various mole ratios (as shown in the diagram) at 650°C after 336 hours of decomposition were superimposed.

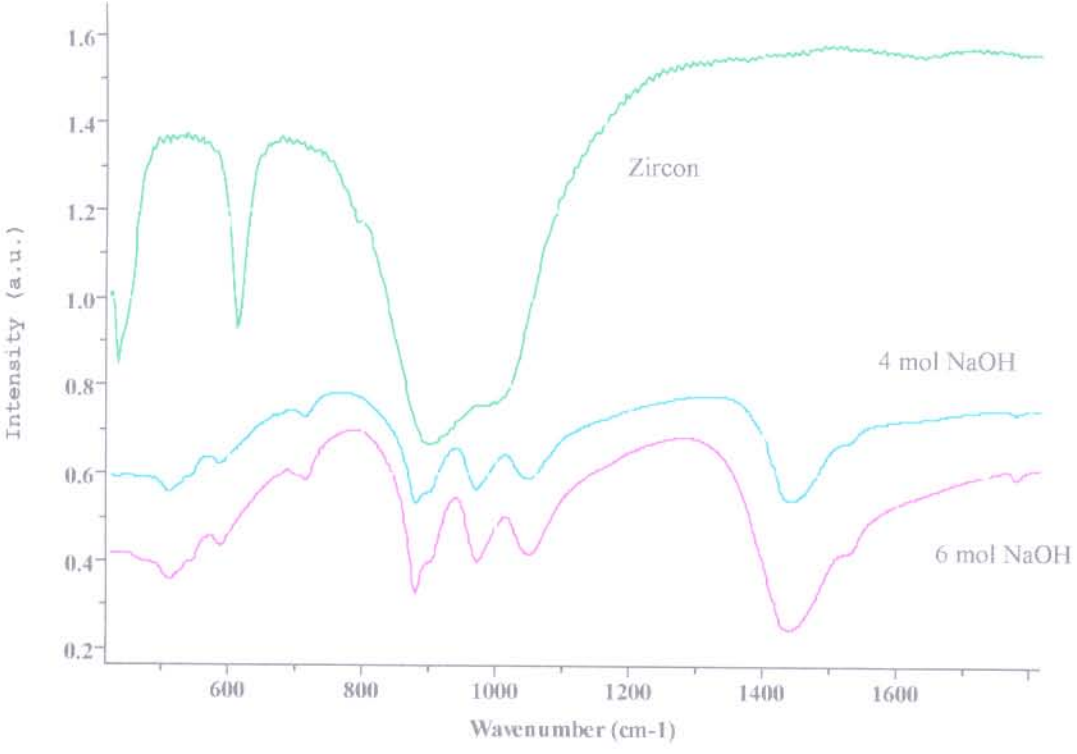

Figure 8.16: A super-positioning of the Infra red spectra of alkali fused decomposed zircon. The spectra at for the various mole ratios (as shown in the diagram) at 650°C after 336 hours of decomposition were superimposed.

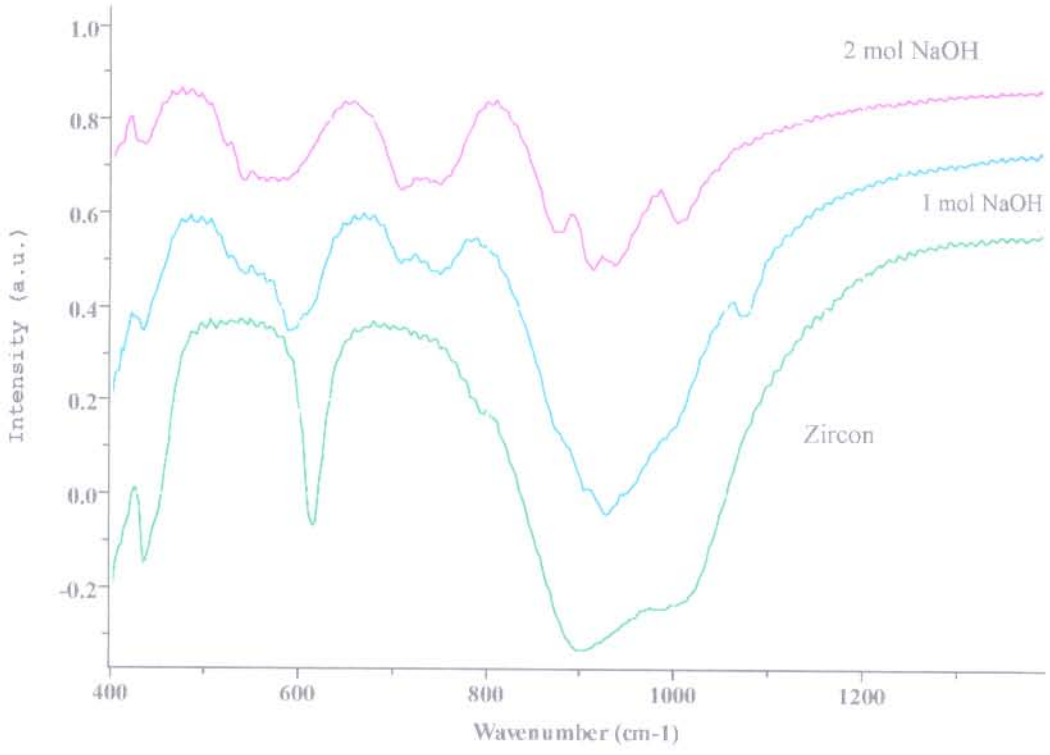

Figure 8.17: A super-positioning of the Infra red spectra of alkali fused decomposed zircon. The spectra at for the various mole ratios (as shown in the diagram) at 850°C after 336 hours of decomposition were superimposed.

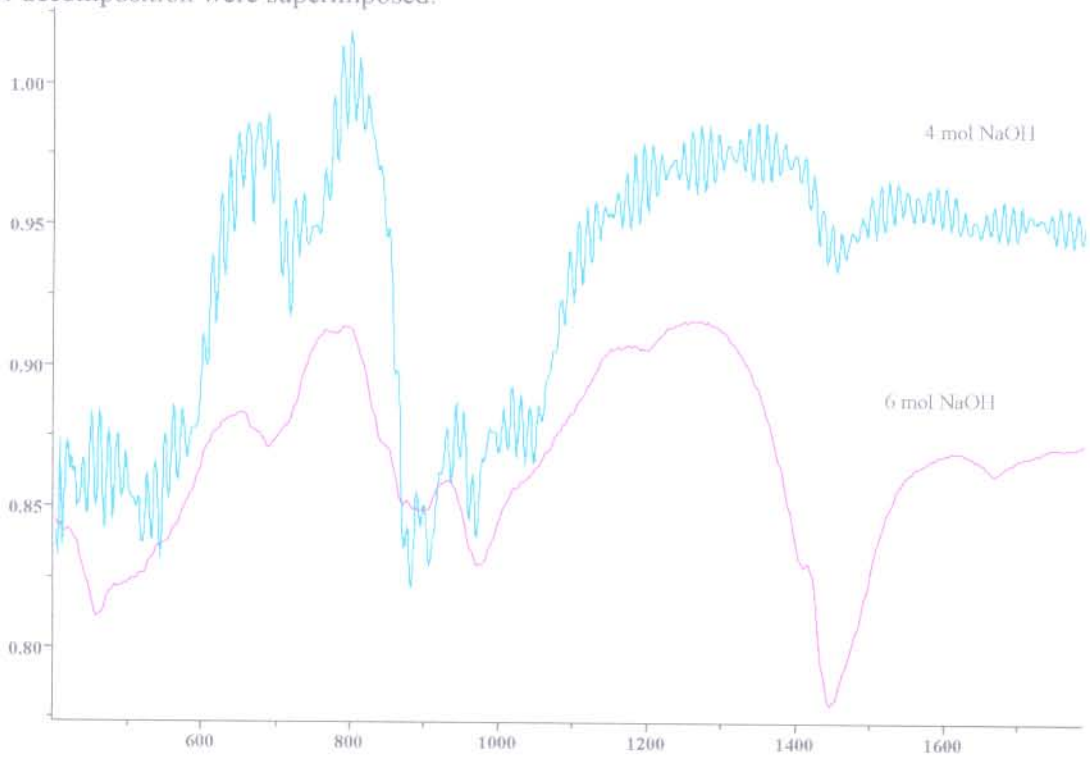

Figure 8.18: A super-positioning of the Infra red spectra of alkali fused decomposed zircon. The spectra at for the various mole ratios (as shown in the diagram) at 850°C after 336 hours of decomposition were superimposed.

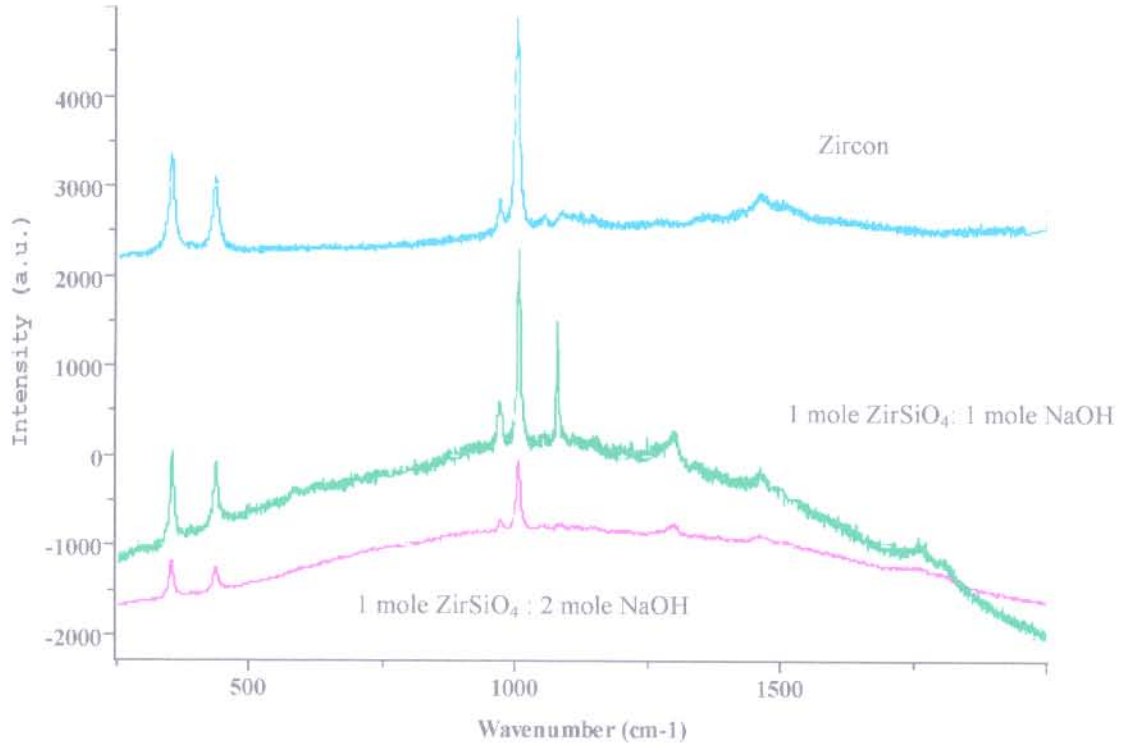

FIGURE 8.19: A Super-positioning of the Raman spectra of alkali fused decomposed zircon. A mole of $d_{50} \approx 9$ μm zircon was decomposed with various moles (as shown on diagram) of sodium hydroxide at 650°C for 336 hours.

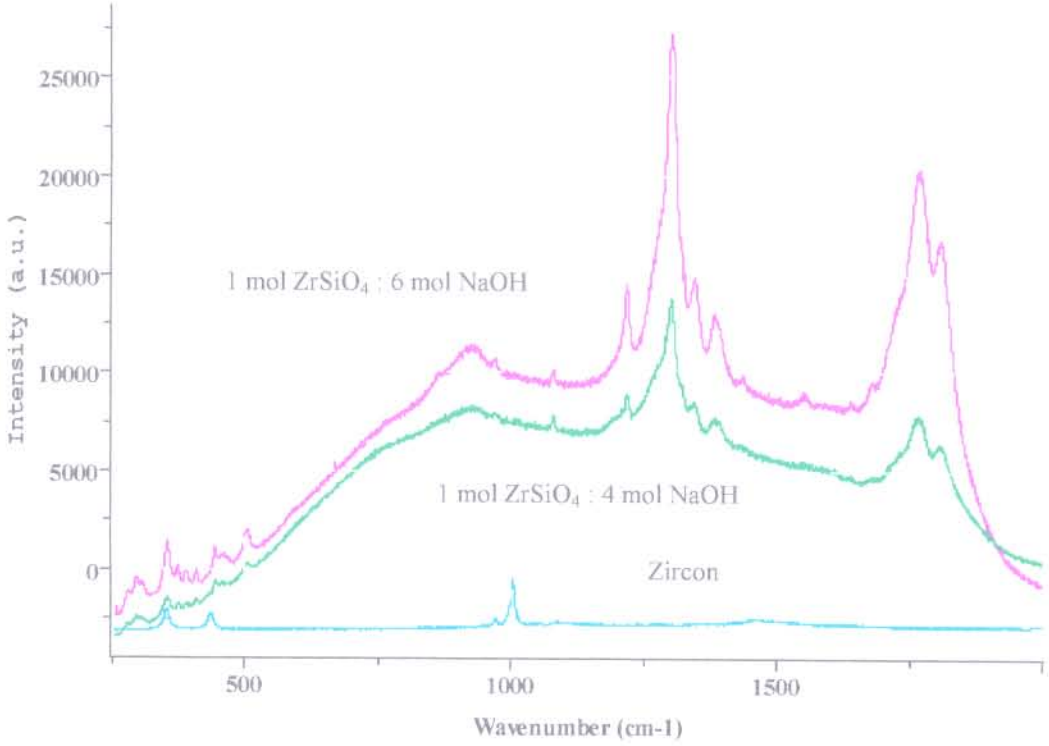

FIGURE 8.20: A Super-positioning of the Raman spectra of alkali fused decomposed zircon. A mole of $d_{50} \approx 9$ μm zircon was decomposed with various moles (as shown on diagram) of sodium hydroxide at 650°C for 336 hours.

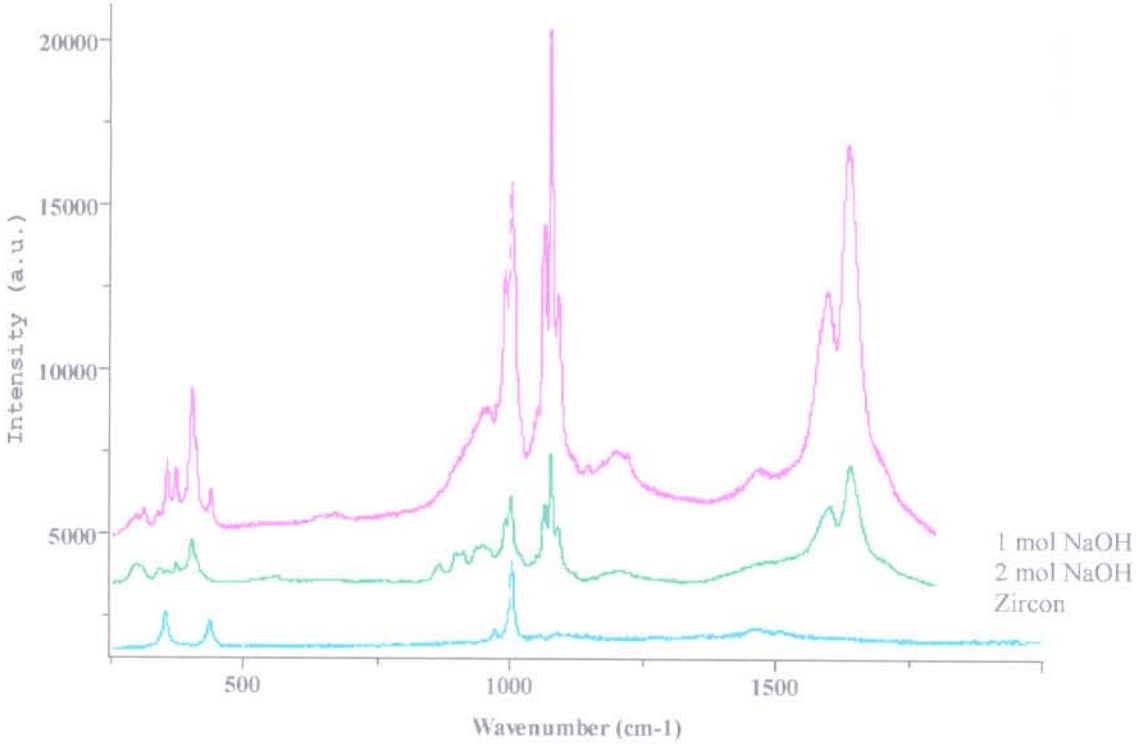

FIGURE 8.21: A Super-positioning of the Raman spectra of alkali fused decomposed zircon. A mole of $d_{50} \approx 9$ μm zircon was decomposed with various moles (as shown on diagram) of sodium hydroxide at 850°C for 336 hours.

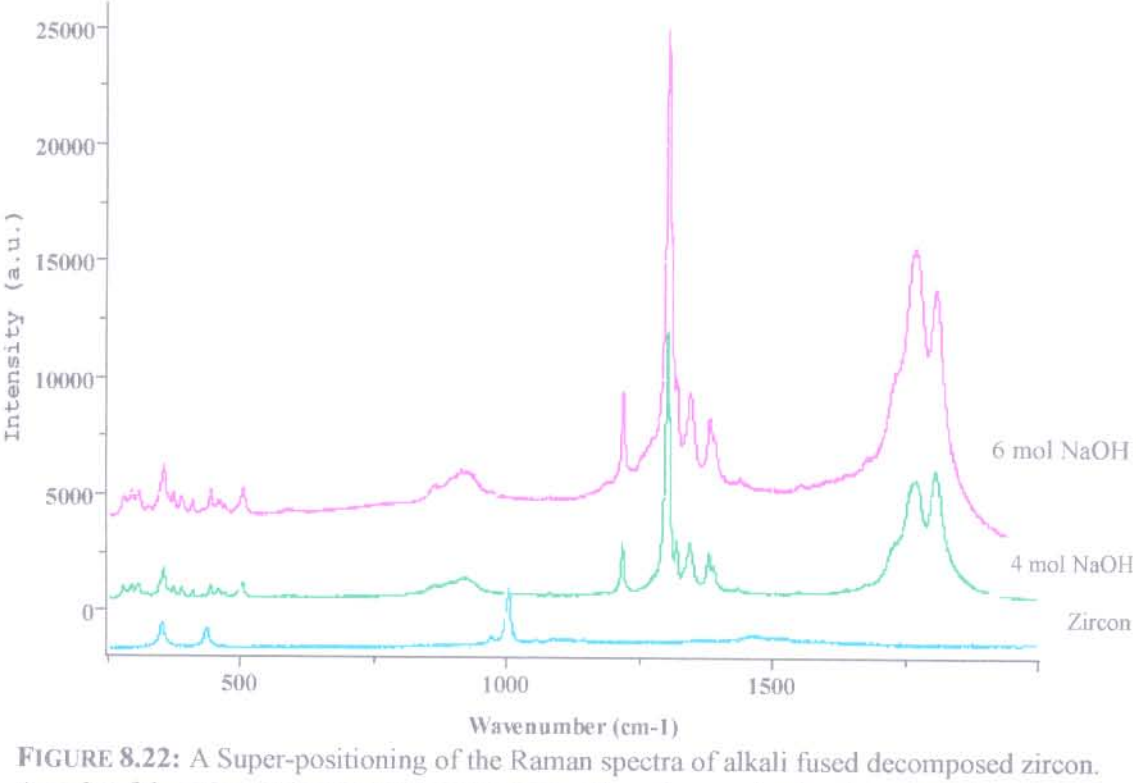

FIGURE 8.22: A Super-positioning of the Raman spectra of alkali fused decomposed zircon. A mole of $d_{50} \approx 9$ μm zircon was decomposed with various moles (as shown on diagram) of sodium hydroxide at 850°C for 336 hours.

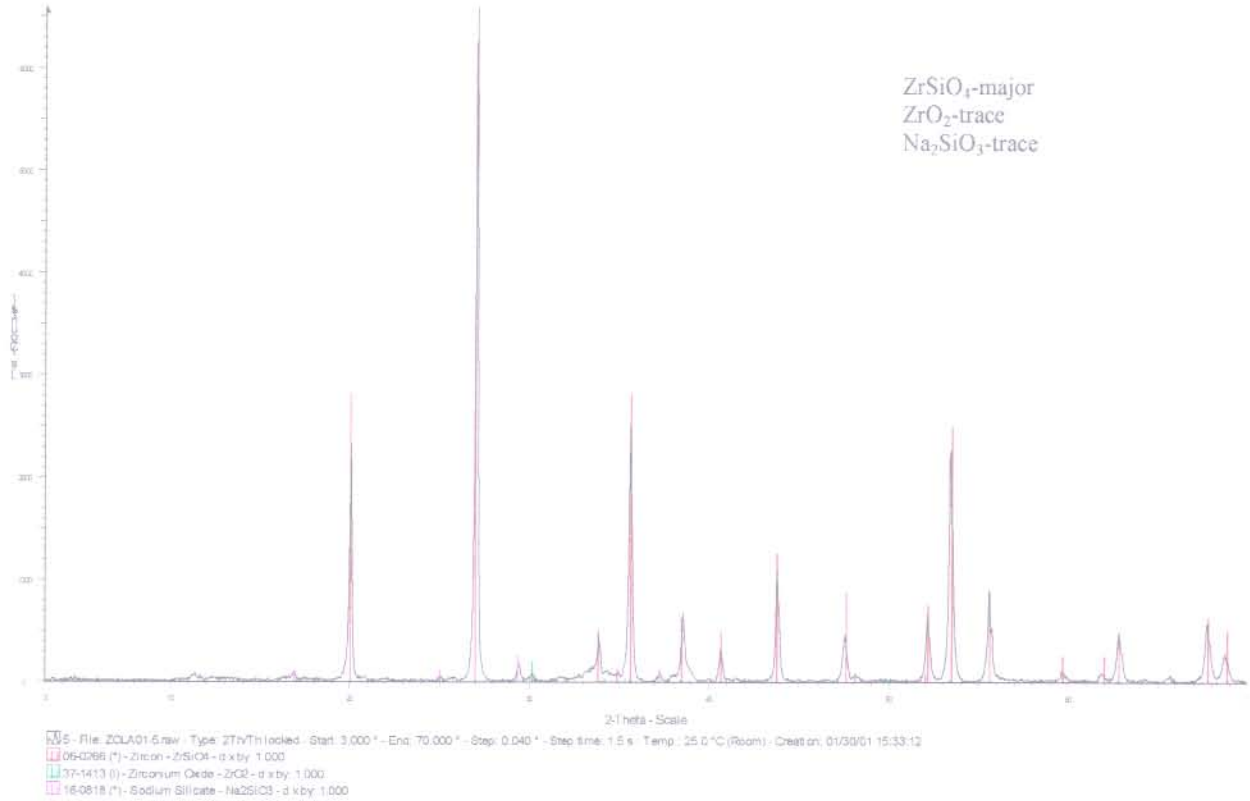

FIGURE 8.23: X-ray diffraction pattern of alkali fused decomposed zircon. A mole of $d_{50} \approx 9\mu m$ zircon was decomposed with a mole of sodium hydroxide at 650°C for 336 hours with intermediate milling after every 24 hours.

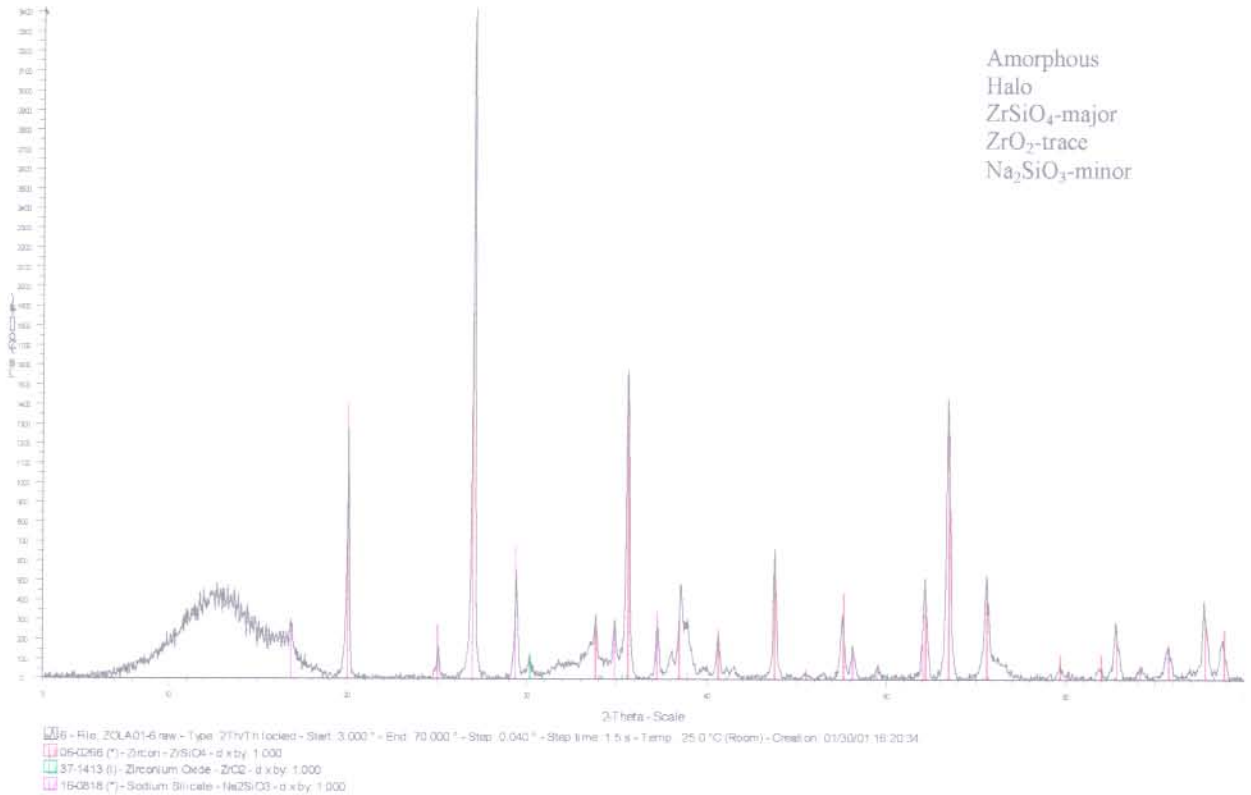

FIGURE 8.24: X-ray diffraction pattern of alkali fused decomposed zircon. A mole of $d_{50} \approx 9\mu m$ zircon was decomposed with two moles of sodium hydroxide at 650°C for 336 hours with intermediate milling after each 24 hours .

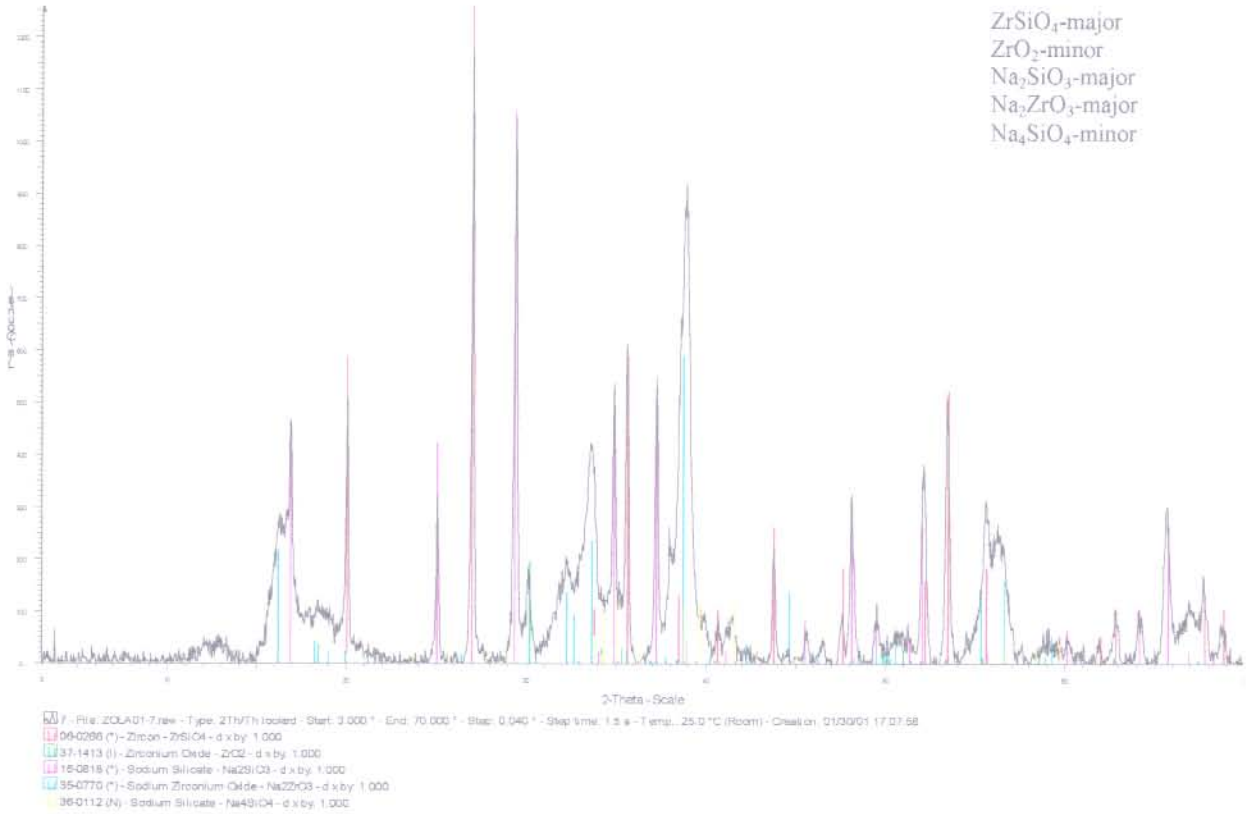

FIGURE 8.25: X-ray diffraction pattern of alkali fused decomposed zircon. A mole of $d_{50} \approx 9\mu m$ zircon was decomposed with four moles of sodium hydroxide at 650°C for 336 hours.

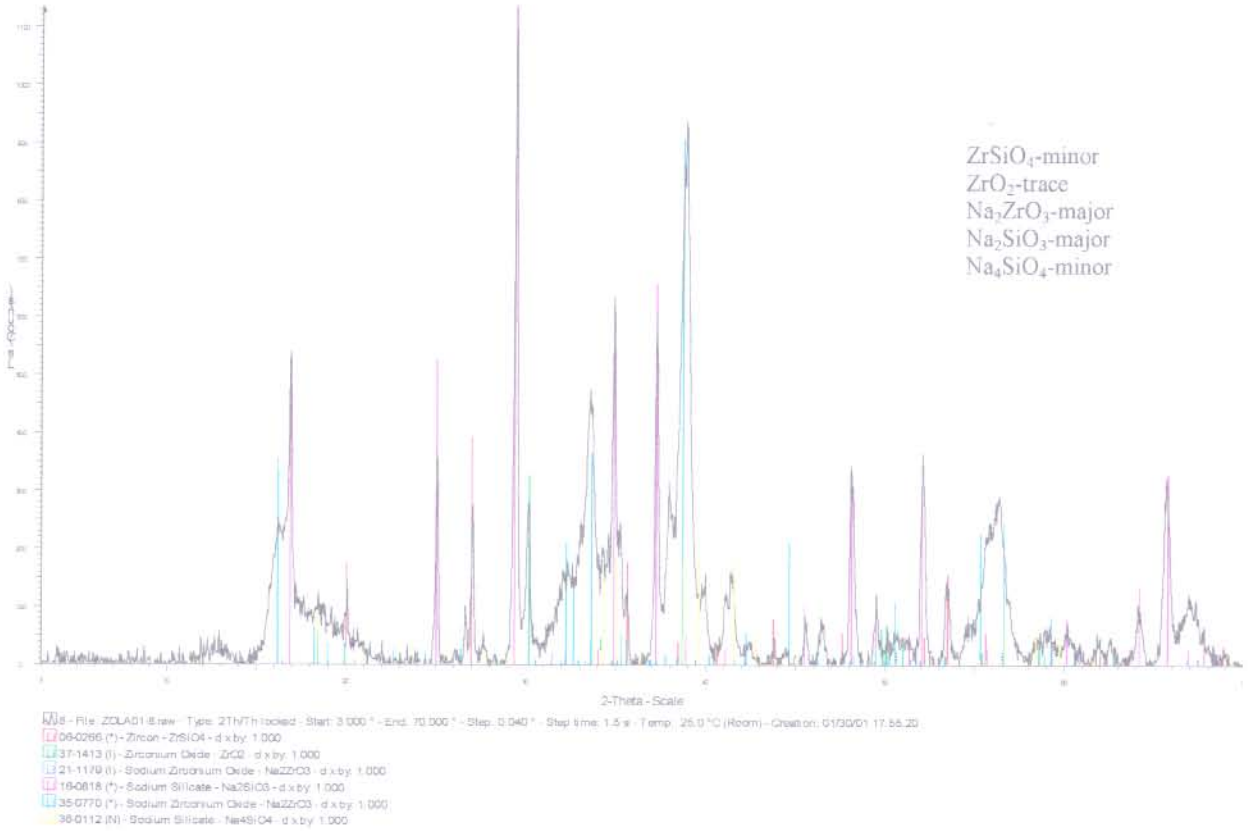

FIGURE 8.26: X-ray diffraction pattern of alkali fused decomposed zircon. A mole of $d_{50} \approx 9\mu m$ zircon was decomposed with six moles of sodium hydroxide at 650°C for 336 hours.

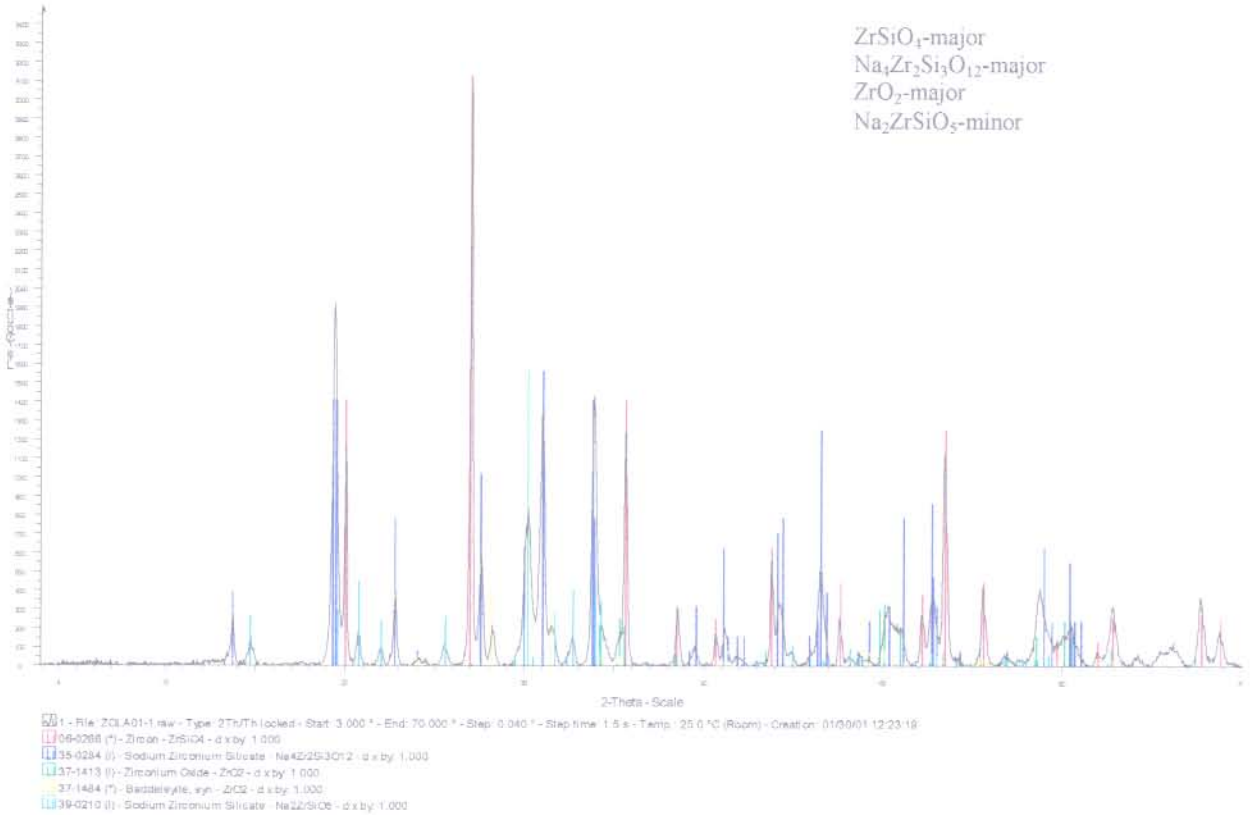

FIGURE 8.27: X-ray diffraction pattern of alkali fused decomposed zircon. A mole of $d_{50} \approx 9$ μm zircon was decomposed with a mole of sodium hydroxide at 850°C for 336 hours.

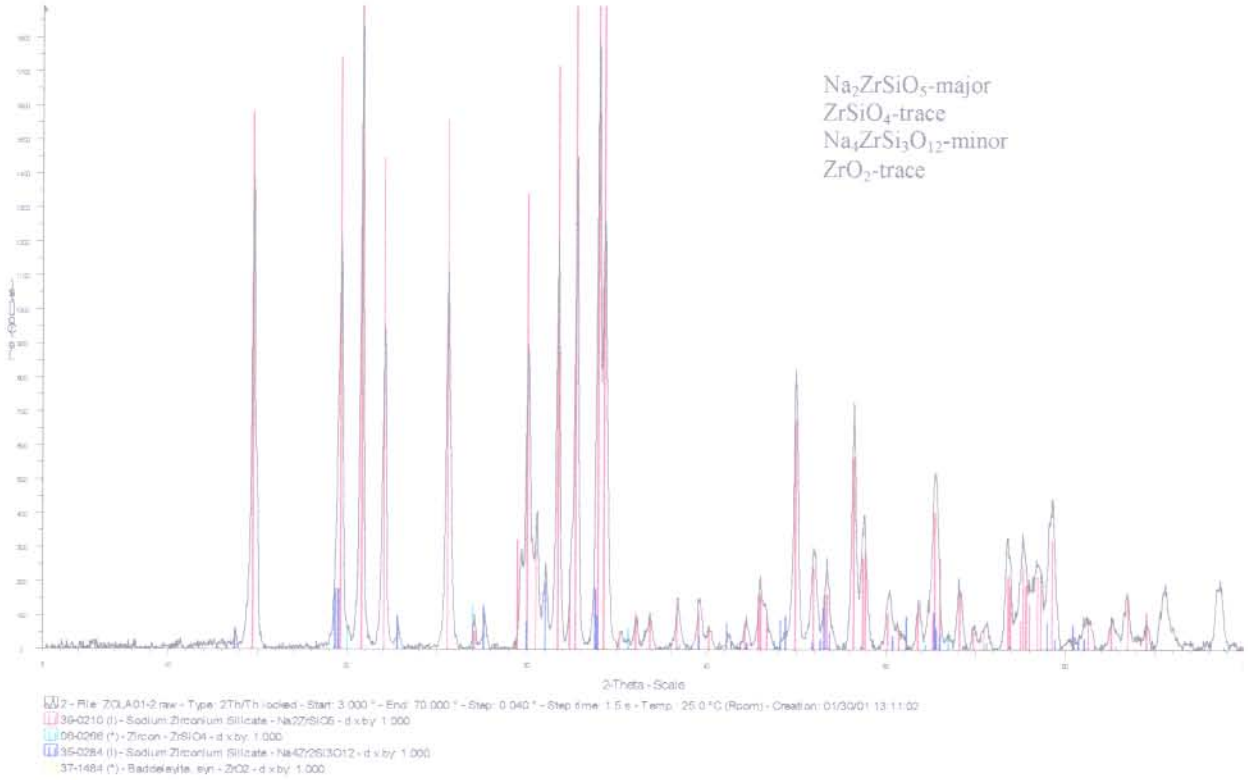

FIGURE 8.28: X-ray diffraction pattern of alkali fused decomposed zircon. A mole of $d_{50} \approx 9$ μm zircon was decomposed with two moles of sodium hydroxide at 850°C for 336 hours with intermediate milling after every 24 hours.

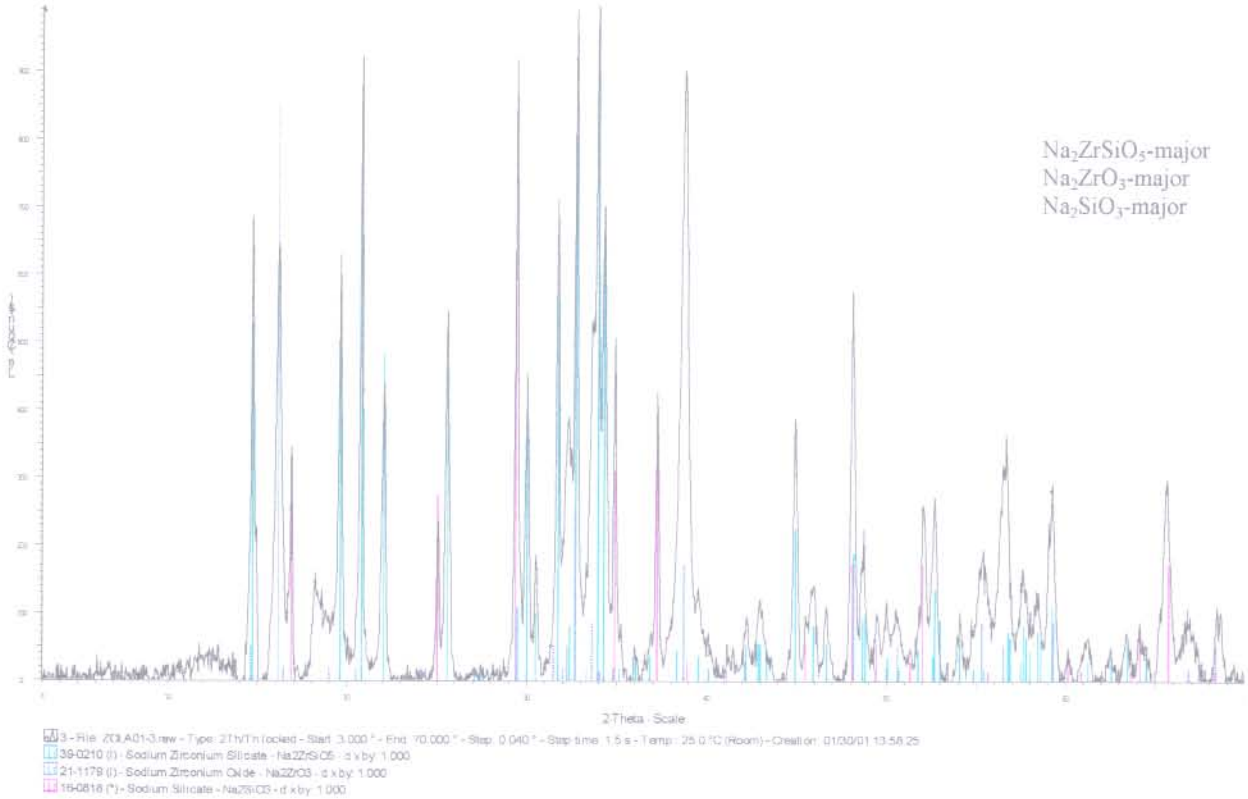

FIGURE 8.29: X-ray diffraction pattern of alkali fused decomposed zircon. A mole of $d_{50} \approx 9\mu m$ zircon was decomposed with four moles of sodium hydroxide at 850°C for 336 hours

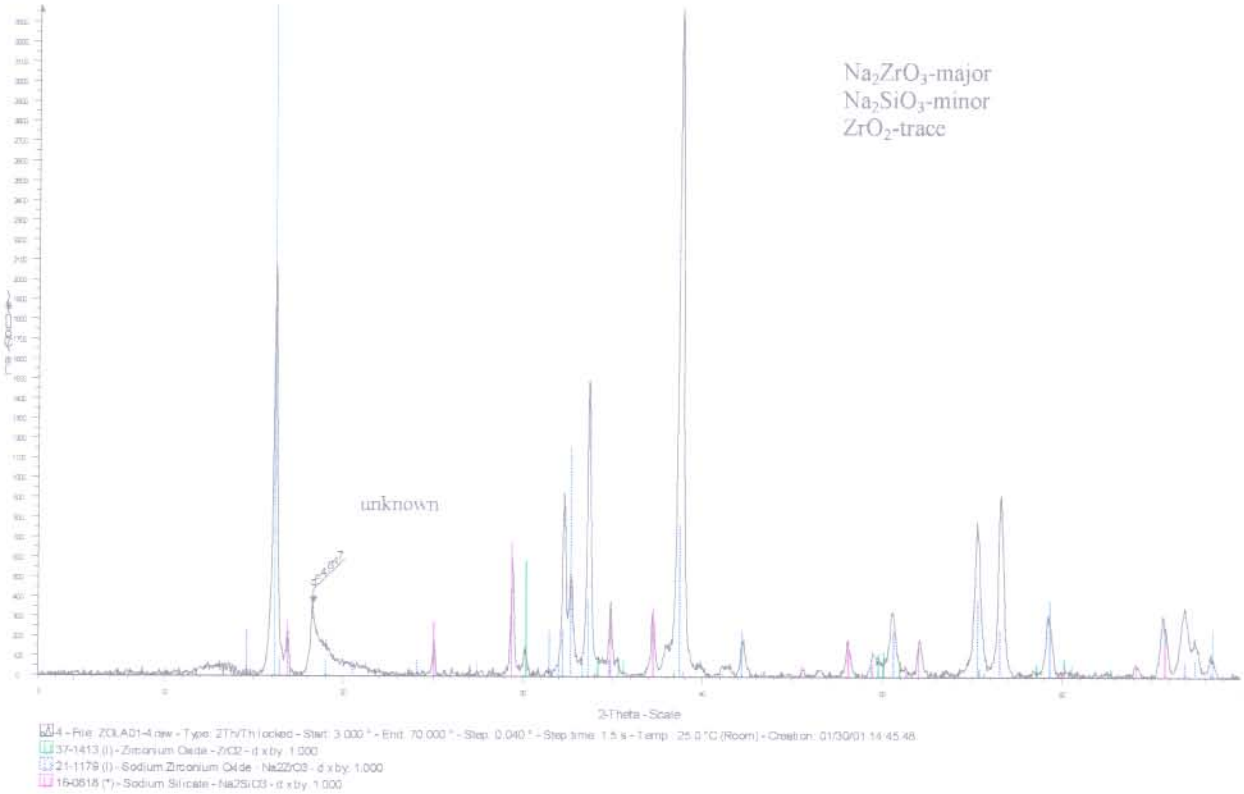

FIGURE 8.30: X-ray diffraction pattern of alkali fused decomposed zircon. A mole of $d_{50} \approx 9\mu m$ zircon was decomposed with six moles of sodium hydroxide at 850°C for 336 hours with intermediate milling after every 24 hours.

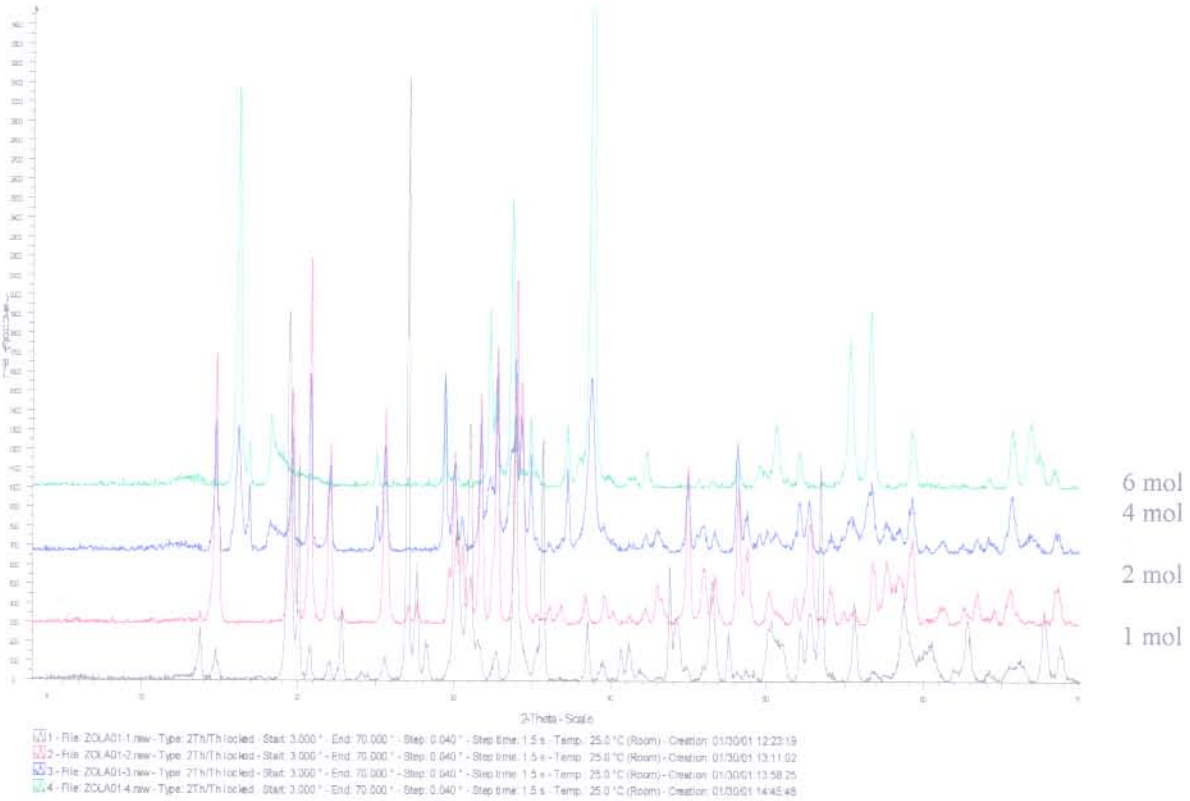

FIGURE 8.31: A super-positioning of the X-ray diffraction pattern of alkali fused decomposed zircon. The spectra at for the various mole ratios at 850°C after 336 hours of decomposition were superimposed.

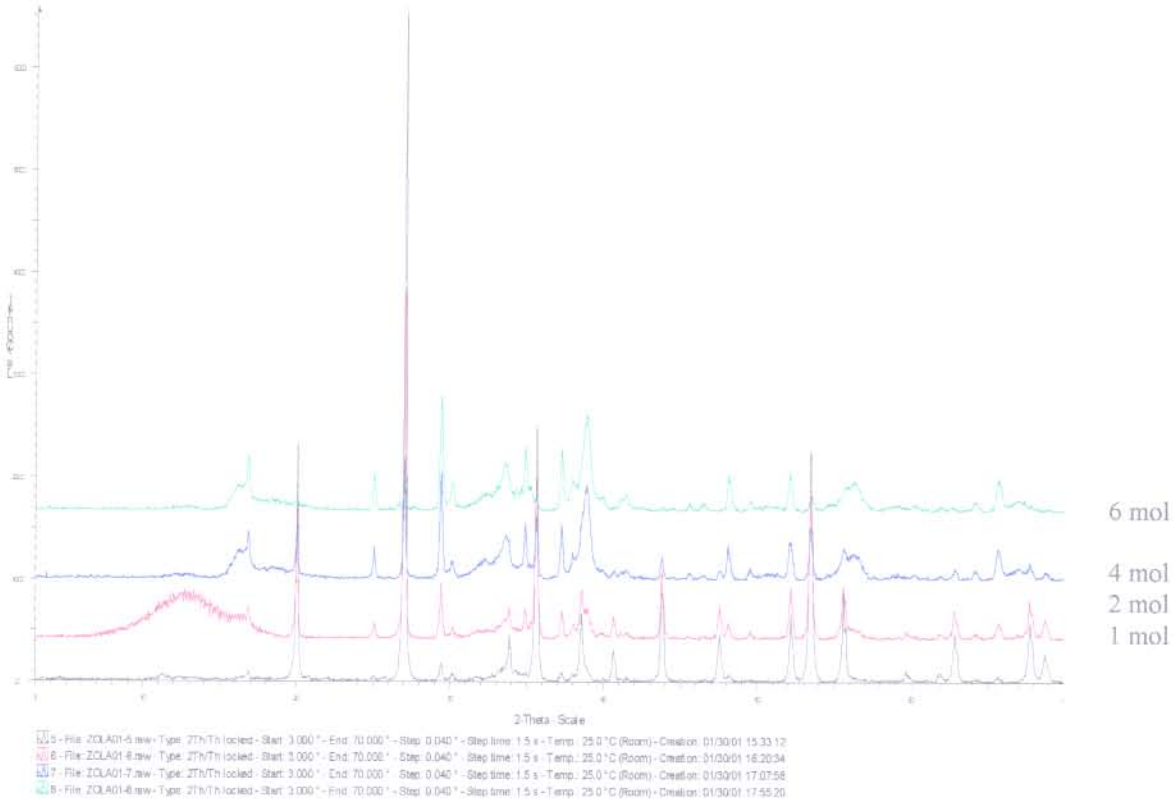

FIGURE 8.32: A super-positioning of the X-ray diffraction pattern of alkali fused decomposed zircon. The spectra for the various mole ratios at 650°C after 336 hours of decomposition were superimposed.

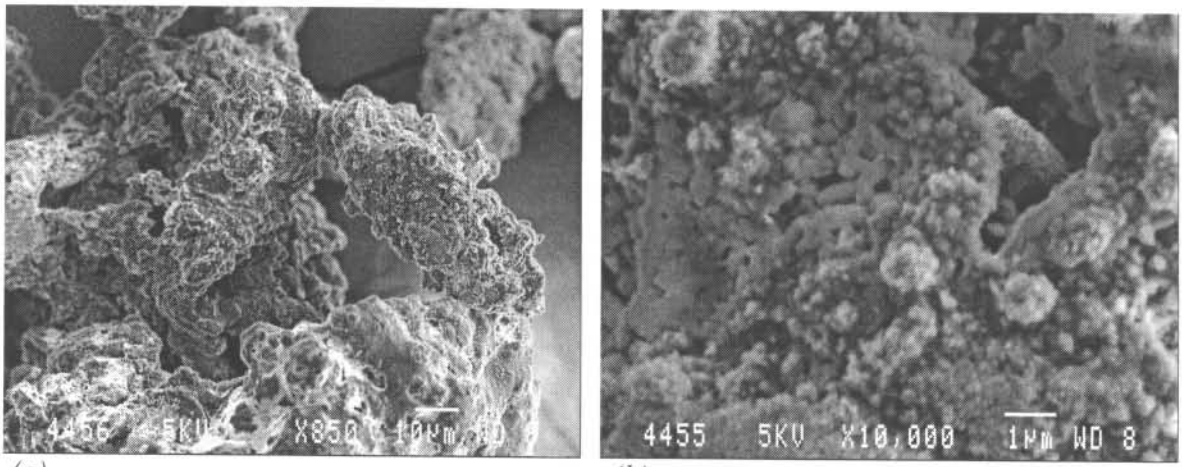

(a) (b)

FIGURE 8.33: SEM photographs of the unmilled by-product sodium metasilicate crystallised overnight by water evaporation in an evaporation oven at 90°C. The by-product was obtained after the water dissolution of AFDZ at 90°C for 5 minutes.

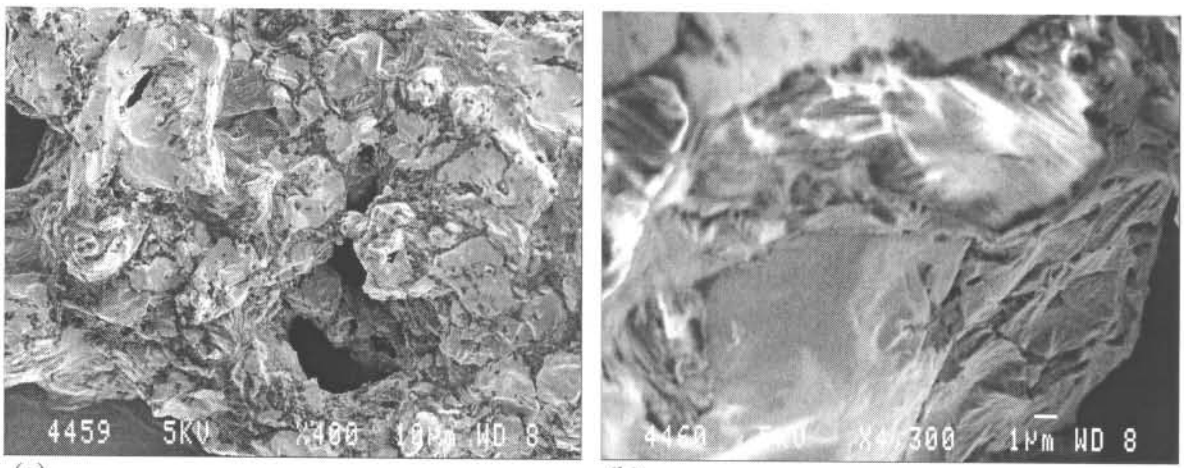

(a) (b)

FIGURE 8.34: SEM photograph of zirconium sulphate tetrahydrate crystallised by water evaporation in a drying oven at 90°C.

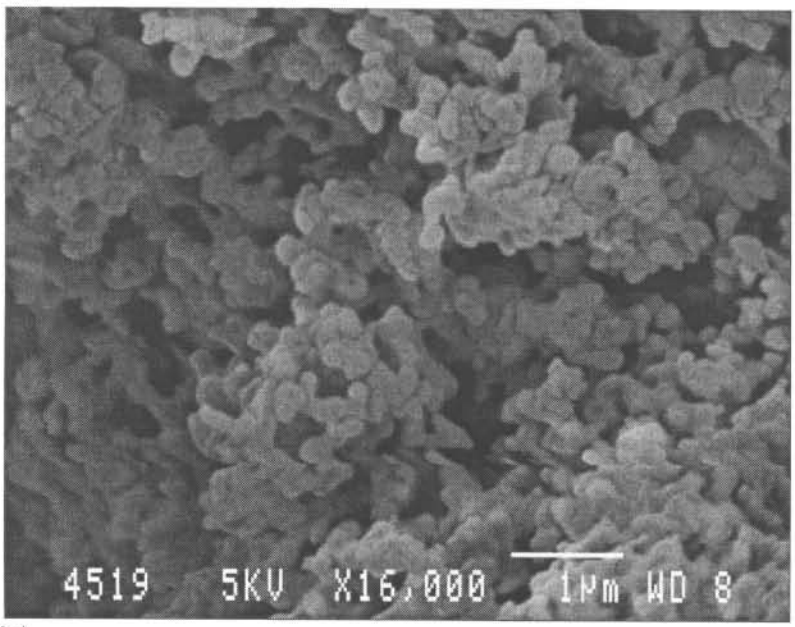

(a)

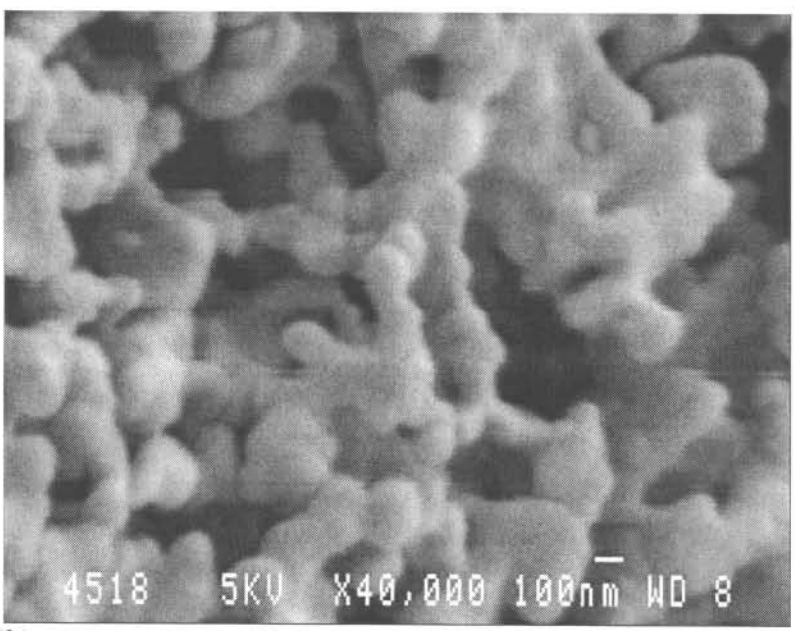

(b)

FIGURE 8.35: SEM photographs of monoclinic zirconia that was obtained by calcining AZST at 900°C for about an hour.

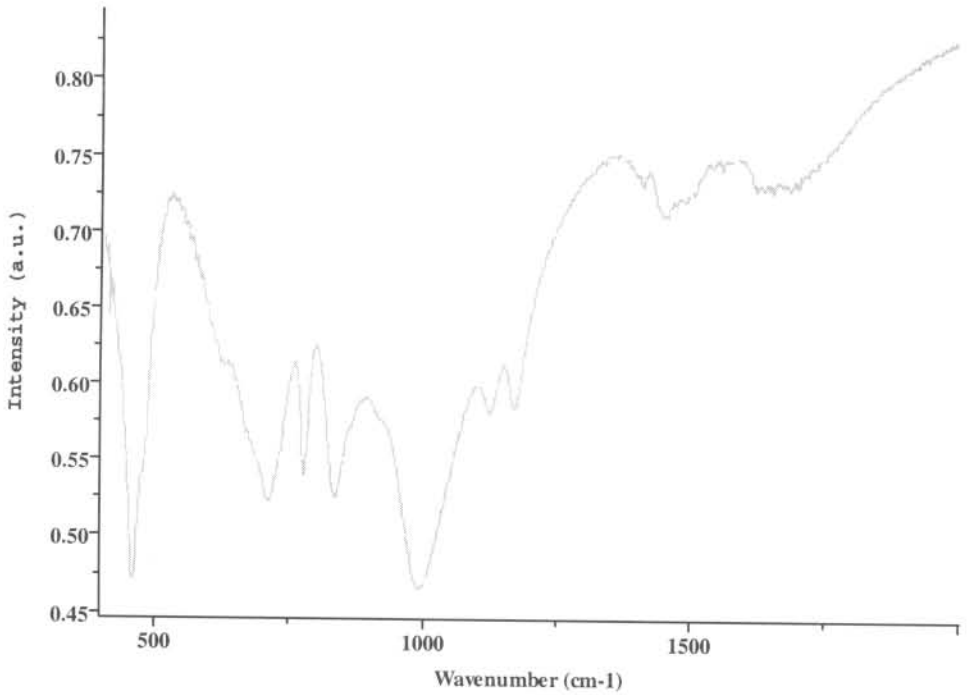

FIGURE 8.36: The infrared spectrum of the sodium silicate by-product. The alkali silicate was crystallised by water evaporation at 90°C overnight.

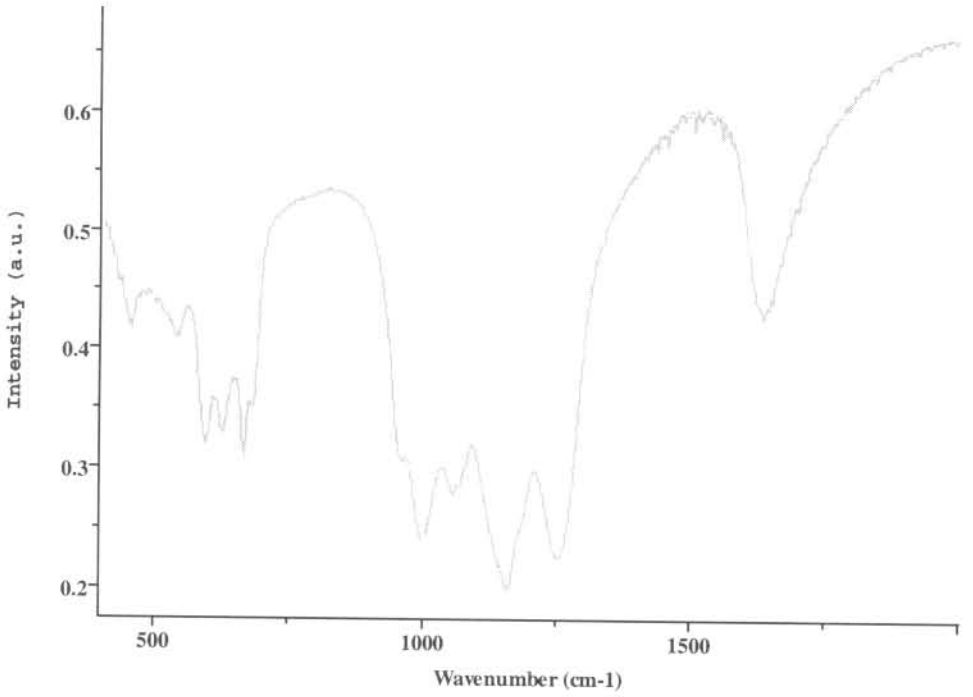

FIGURE 8.37: The infrared spectrum of zirconium sulphate tetrahydrate. The sulphate was crystallised by water evaporation at 90°C overnight.

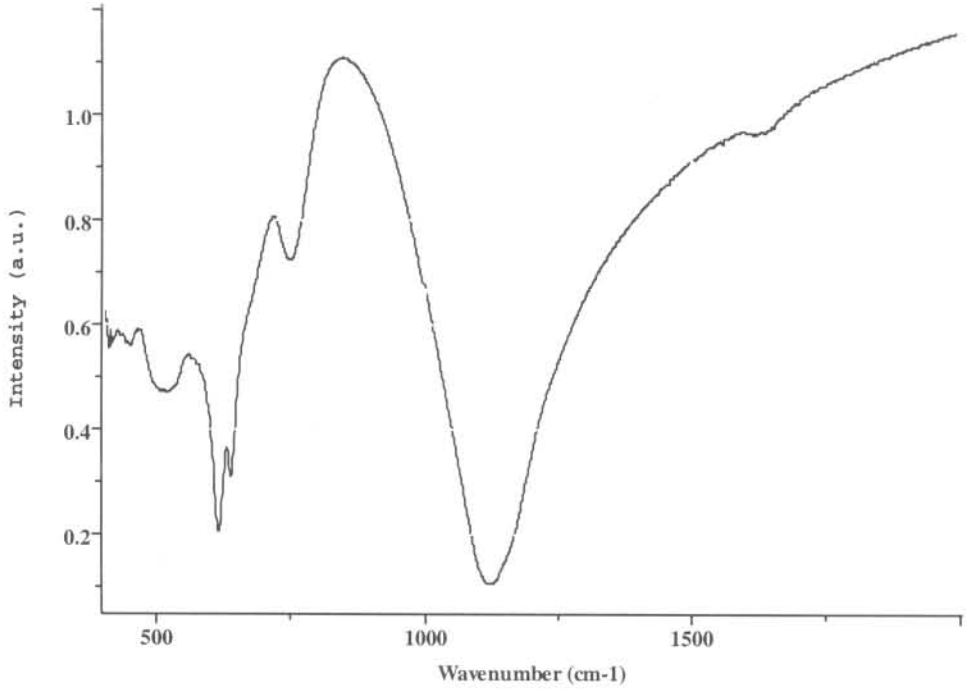

FIGURE 8.38: The infrared spectrum of zirconia. The zirconia was obtained by calcining AZST at 900°C for an hour.

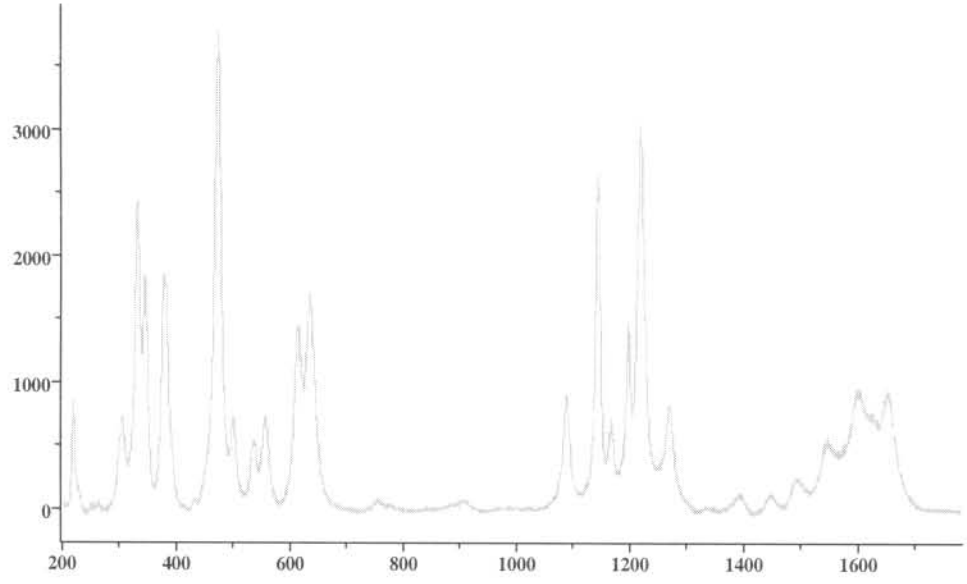

FIGURE 8.39: The Raman spectrum of monoclinic zirconia. The zirconia was obtained by calcining AZST at 900°C for an hour.

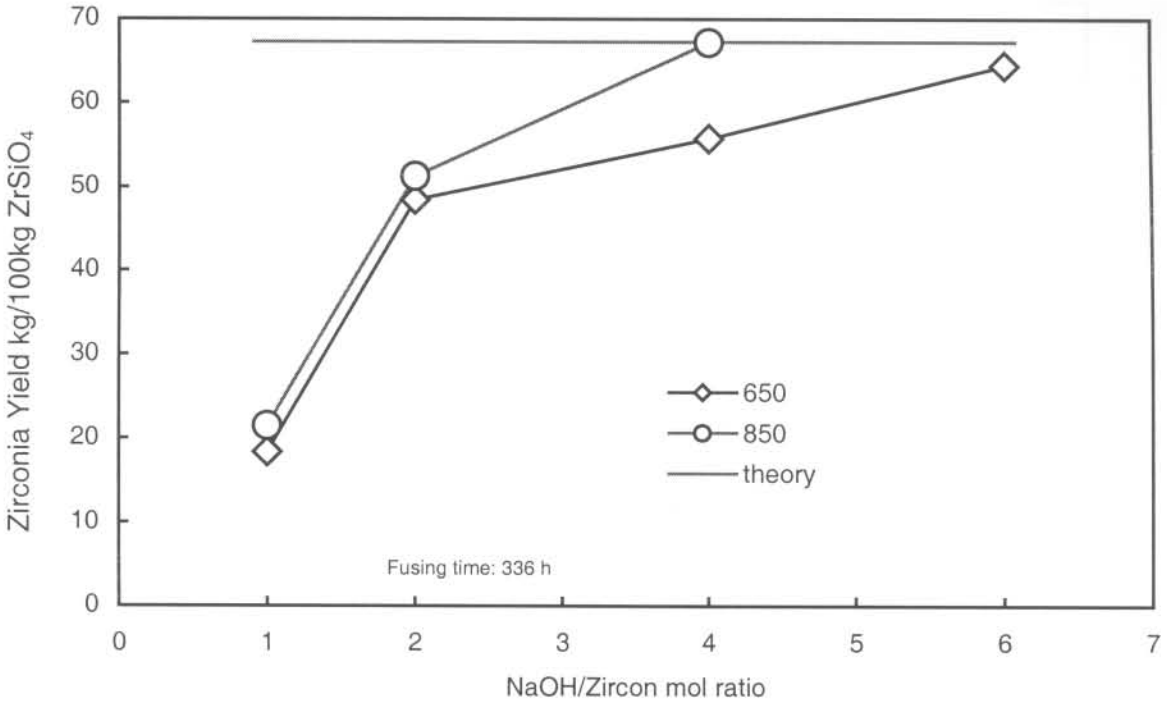

FIGURE 8.40: The influence of the moles of sodium hydroxide on the yield of zirconia. The values given are those used in a mass balance; the zirconia was obtained from AFDZ that was fused for 336 hours with intermediate milling.

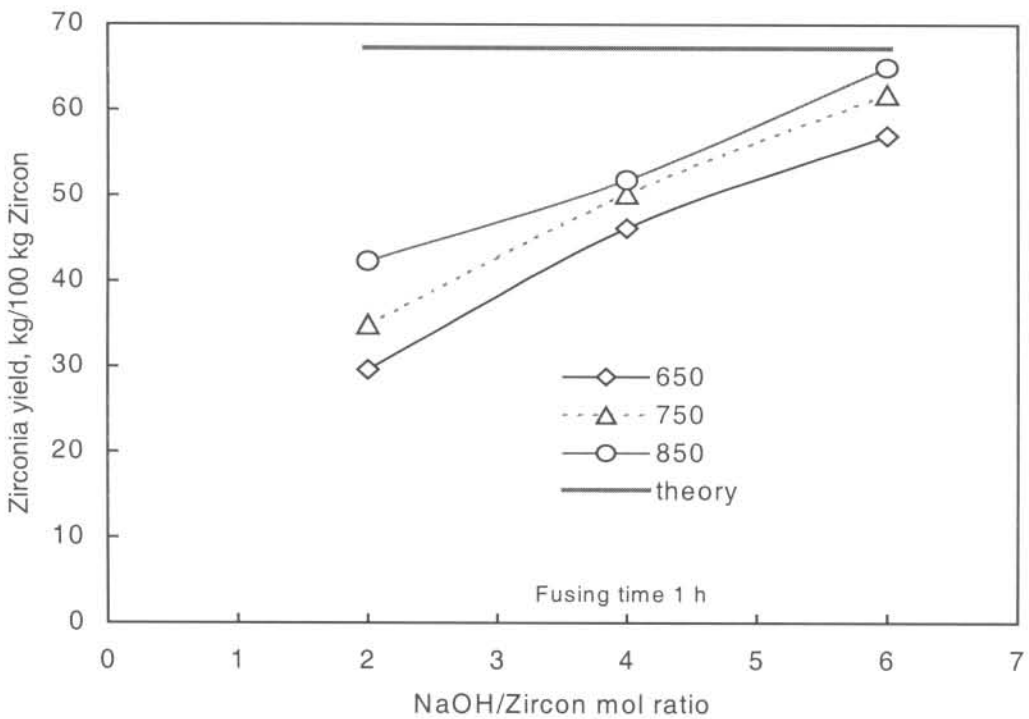

FIGURE 8.41: The influence of the moles of sodium hydroxide on the yield of zirconia. The values given are those used in a mass balance; the zirconia was obtained from AFDZ that was fused for one hour with intermediate milling.

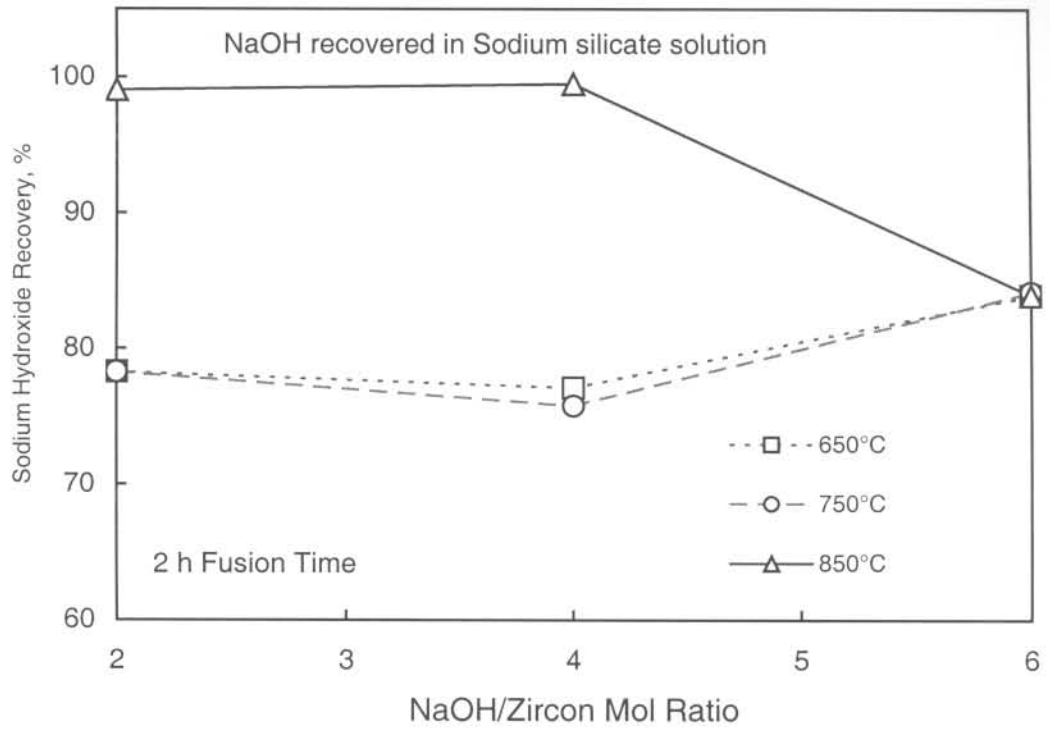

FIGURE 8.42: The influence of sodium hydroxide to zircon mole ratio on the amount of sodium recovered from solids fused for 2 hours. The sodium was recovered with soluble sodium silicates.

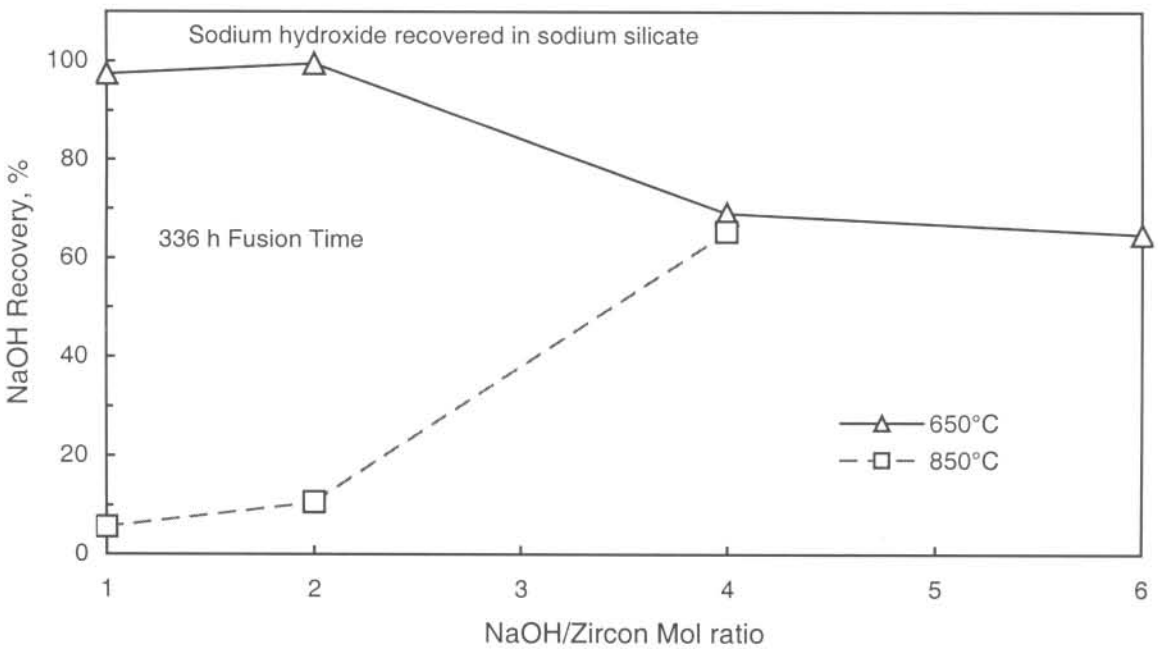

FIGURE 8.43: The influence of sodium hydroxide to zircon mole ratio on the amount of sodium recovered from solids fused for 336 hours. The sodium was recovered with soluble sodium silicates.

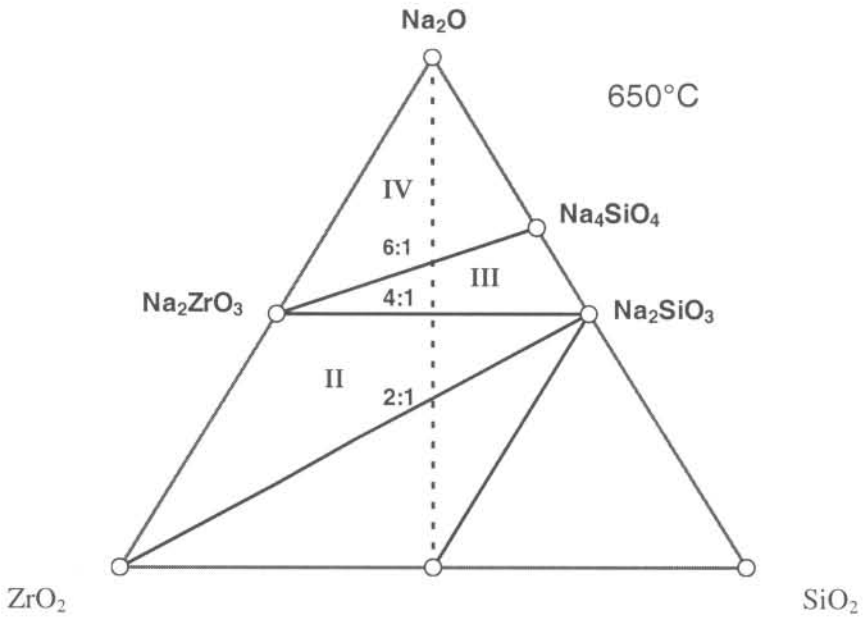

FIGURE 8.44: A diagrammatic representation of the phase diagram obtained for the decomposition of zircon with sodium hydroxide at 650°C. The phases Na_2ZrSiO_5 and $Na_4Zr_2Si_3O_{12}$ were not observed.

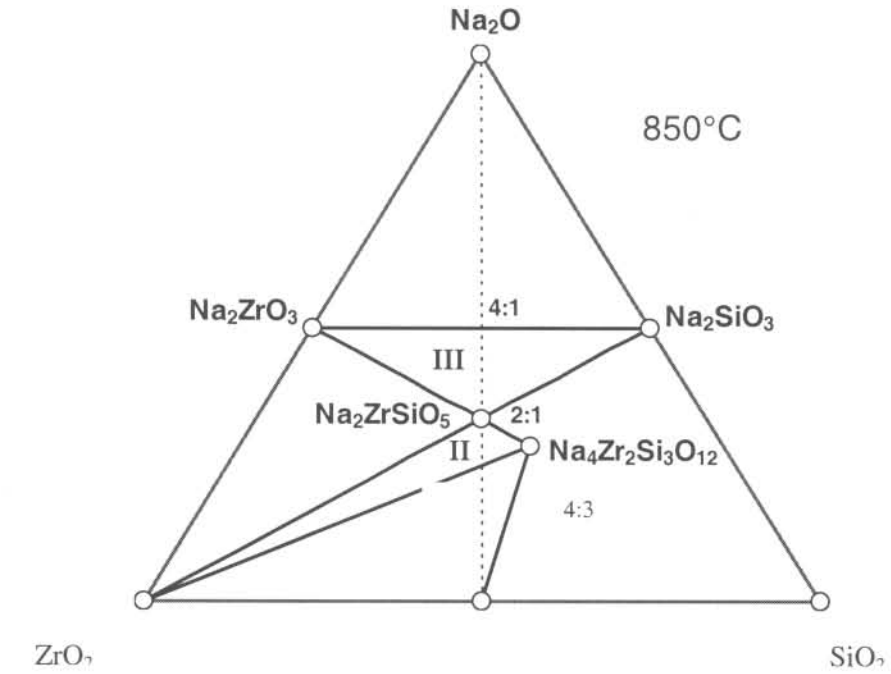

FIGURE 8.45: A diagrammatic representation of the phase diagram obtained for the decomposition of zircon with sodium hydroxide at 850°C. The phases Na_2ZrSiO_5 and $Na_4Zr_2Si_3O_{12}$ were observed. The diagram is comparable to that by D' Ans and Loeffer (1930).

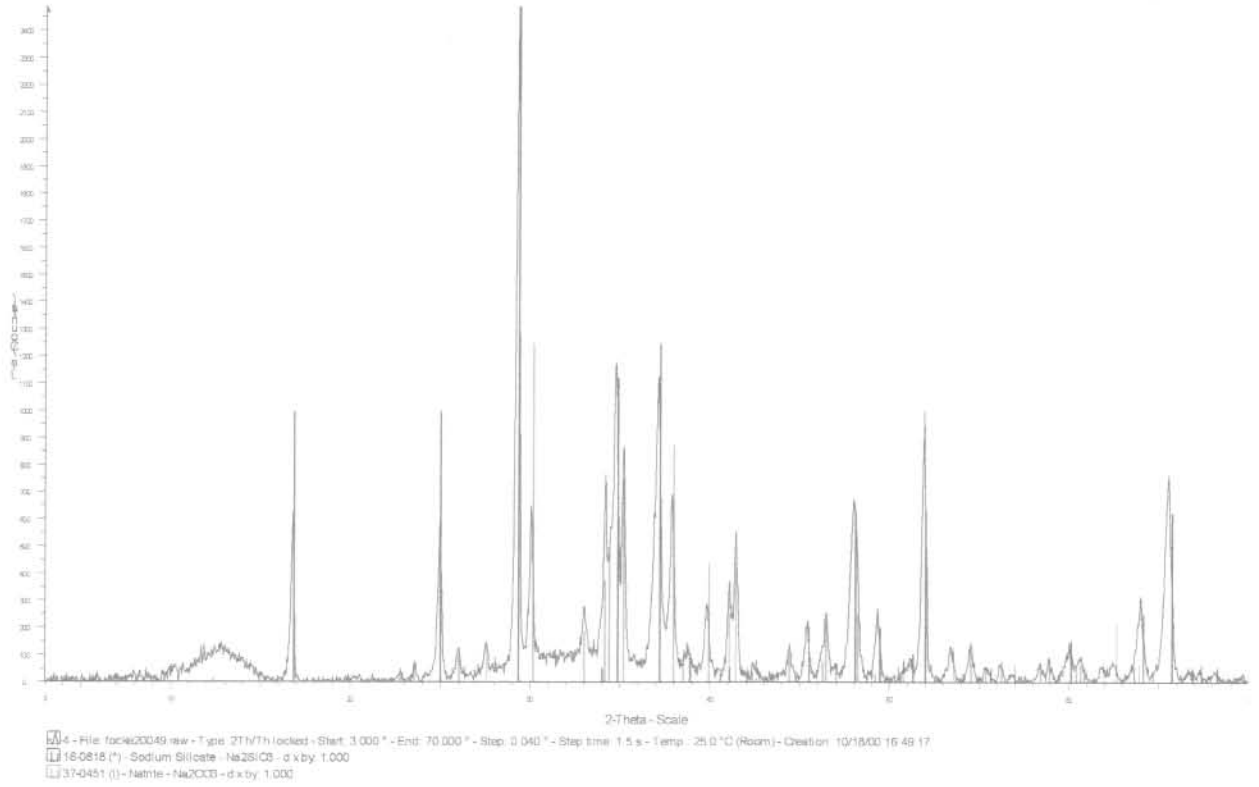

FIGURE 8.46: X-ray diffraction pattern of the alkali silicate by-product. The silicate was crystallised by water evaporation at 90°C overnight.

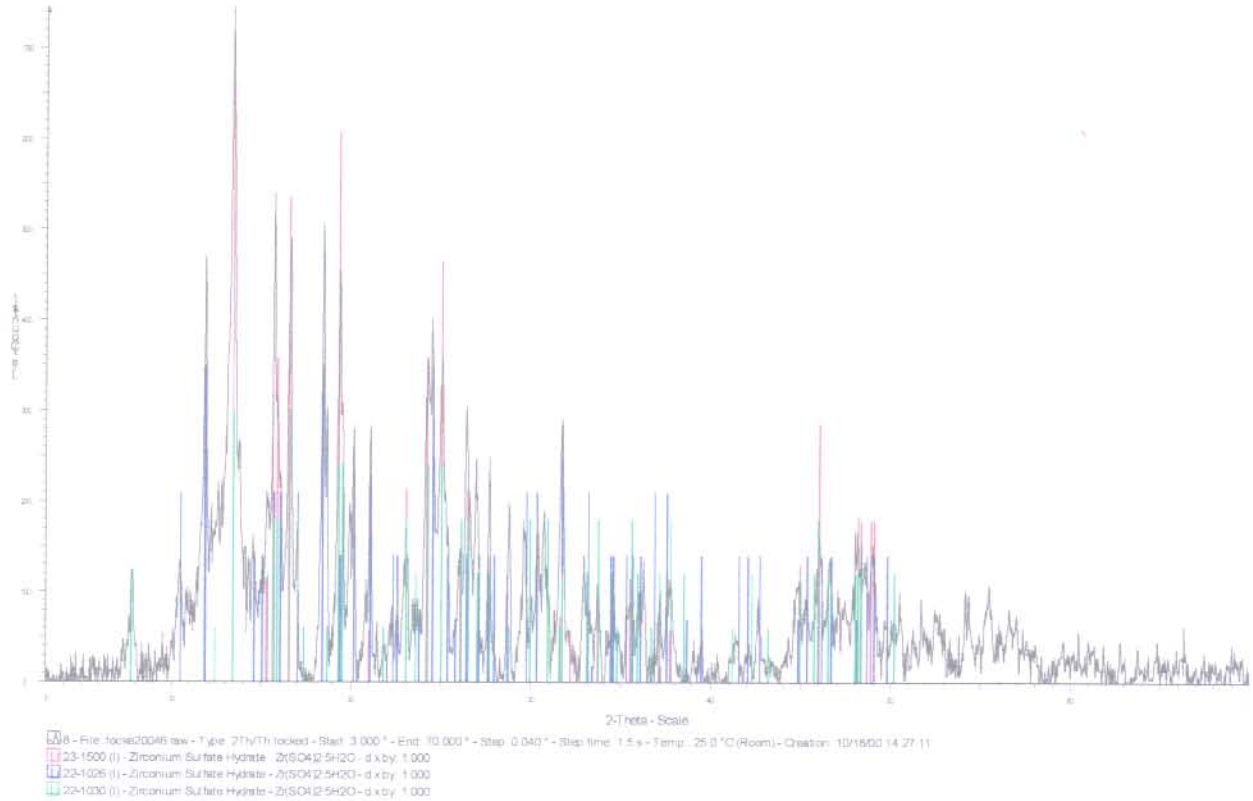

FIGURE 8.47: X-ray diffraction pattern of zirconium sulphate, AZST. The hydrated normal sulphate was crystallised by water evaporation at 90°C overnight.

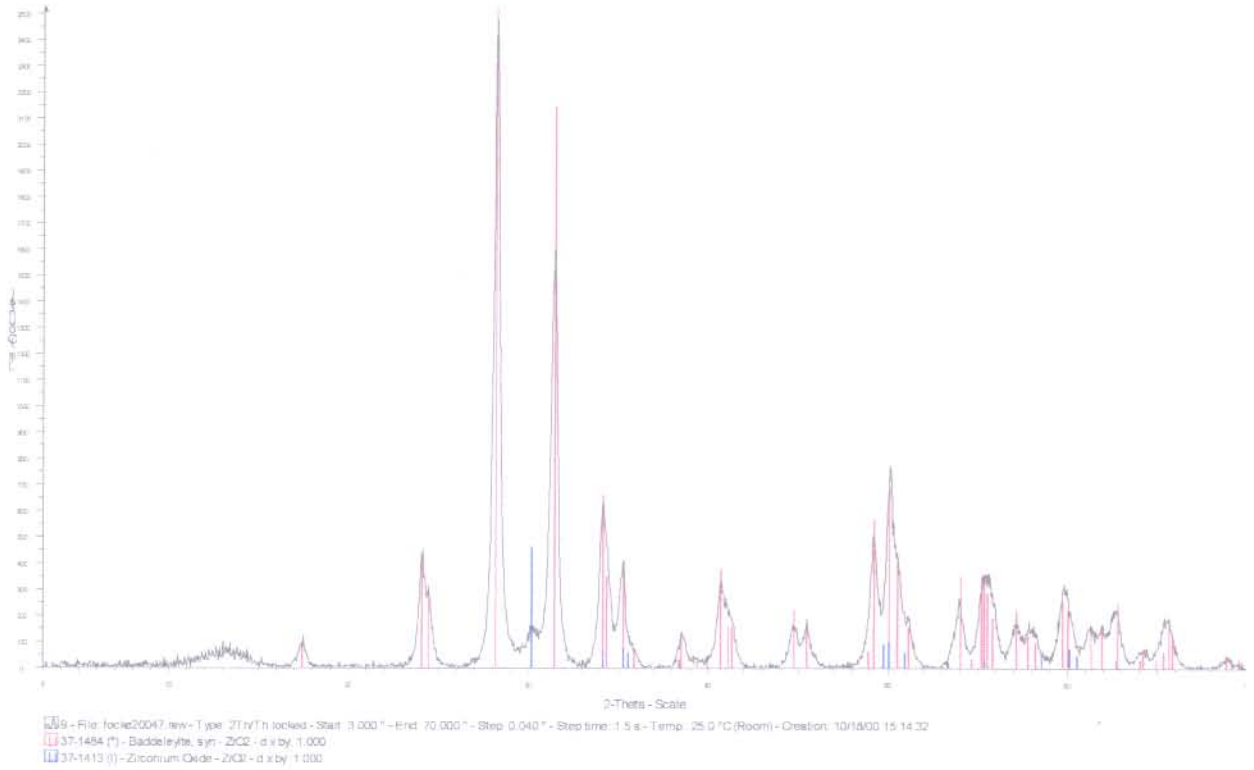

FIGURE 8.48: X-ray diffraction pattern of zirconia. The zirconia was obtained by calcining AZST at 900°C for about an hour.

8.3 DISCUSSIONS

8.3.1 ZIRCON DECOMPOSITION AFTER TWO HOURS OF FUSION

Figure 8.1 shows SEM photographs of milled zircon sand from Richard's bay, South Africa. Figure 8.1 (a) is a photograph of the $d_{50} \approx 45\mu m$ zircon sand and Figure 8.1 (b) is the $d_{50} \approx 9\mu m$ sand. The difference in the particle size can be seen in the SEM photographs. Appendix K provides the XRF determined elemental analysis of this product.

Figure 8.2 shows the fusion product commonly called alkali fusion decomposed zircon (AFDZ). The $d_{50} \approx 9\mu m$ zircon sand was decomposed with sodium hydroxide at various mole ratios and temperature. Figure 8.2 (a) shows the size of an agglomerate of AFDZ. A closer look at the surface of the agglomerate, Figure 8.2 (b), shows a large (c.a. 25μm) molten region (melt). The melt could possibly be unreacted Na_2O. The SEM suggests that there was segregation of reactants during fusion. The NaOH melts at approximately 324°C before zircon at approximately 2 200°C. The higher sodium content of the melt was verified by X-ray analysis with the aid of the SEM. This region was seen for all AFDZ samples that were not *intermediately* milled.

This segregation can be minimised by milling followed by a second fusion step. The advantage is improved zircon decomposition (zirconia yields improved by 10-15%). The disadvantages are long process times and the additional processing step (milling).

Figures 8.3 to 8.5 show the infrared spectra of AFDZ at various reaction conditions. New bands appear at 686, 864, 1 410, 1 669 and 1 756 cm^{-1}. These bands increase in intensity as the sodium hydroxide to zircon mole ratio is increased. With increase of temperature, the intensity of the new bands decreases. For the fusion of a mole of zircon with six moles NaOH, the bands observed at 650°C had minimal intensity at 850°C. As shown below, XRD aided the interpretation of the infrared spectra.

Figure 8.6 shows the XRD spectra of milled zircon sand from Richard's bay. The spectra for the 9 and 45 μm are similar. There appears to be a small amorphous halo in the spectra.

Figures 8.7 to 8.14 show the XRD patterns of the AFDZ at 850°C and 650°C for the various mole ratios when fused for two hours. The AFDZ went through a single cycle of milling and fusion to obtain a homogenous mixture. The relative intensities in the XRD spectra are given in brackets.

Figure 8.7 shows the XRD pattern for the fusion of a mole of zircon with two moles of sodium hydroxide at 850°C. The phases Na_2ZrSiO_5 (major), Na_2ZrO_3 (minor) unreacted $ZrSiO_4$ (major) and traces of Na_2SiO_3 were observed. Zircon is the major component, suggesting that its decomposition is incomplete. The infrared spectrum is also dominated by bands due to zircon.

Figure 8.8 shows the XRD pattern for the fusion of a mole of zircon with four moles of sodium hydroxide at 850°C. The phases Na_2ZrSiO_5 (trace), Na_2SiO_3 (minor), different phases of Na_2ZrO_3 (major) were observed. The zircon ($ZrSiO_4$) was identified in trace amount only indicating virtually complete zircon decomposition.

Figure 8.9 shows the XRD pattern for the fusion of a mole of zircon with six moles of sodium hydroxide at 850°C. The phases Na_2ZrSiO_5 (minor), different phases of Na_2ZrO_3 (major), and traces of ZrO_2 and $ZrSiO_4$ were observed. The zircon was identified in trace amounts only. It indicates that this reaction condition provides for complete zircon decomposition.

At the 2 hour stage of fusion at 850°C, the XRD spectra suggest that increments of NaOH improve the decomposition of zircon. Near complete zircon decomposition is obtained when fusing a mole of zircon with four moles of NaOH. When fusing a mole of zircon with two moles of NaOH the phase Na_2ZrSiO_5 is obtained in majority, but with increments of NaOH the phase is formed in minority. The quantity of Na_2ZrO_3 and Na_2SiO_3 are seen to increase with increments of NaOH.

Figure 8.11 shows the XRD pattern for the fusion of a mole of zircon with two moles of sodium hydroxide at 650°C. The phases Na_2ZrO_3 (trace), $ZrSiO_4$ (major), Na_2SiO_3 (trace) and ZrO_2 (trace) were observed. Zircon was the major phase; this amount suggests a small extent of decomposition.

Figure 8.12 shows the XRD pattern for the fusion of a mole of zircon with four moles of sodium hydroxide at 650°C. The phases Na_2ZrO_3 (minor), ZrO_2 (minor), ZrO (major) and $ZrSiO_4$ (major) were observed. No sodium silicates were detected. The presence of the amorphous halo indicates that the sample was amorphous, possibly explaining the poor detection of sodium silicates. The detection of the phase ZrO in majority suggests the preference of sodium to attack the less stable silica tetrahedral linkages. The zirconia could have been reduced by the decomposition by-product, water.

Figure 8.13 shows the XRD pattern for the fusion of a mole of zircon with six moles of sodium hydroxide at 650°C. The XRD spectrum indicates the presents of sodium silicates high in sodium content Na_4SiO_4 (minor), $Na_6Si_2O_7$ (minor) and traces of $Na_2Si_2O_5$ (low in sodium). The phase ZrO is identified in majority. Zircon and zirconia are other phases identified in minority. The presents of the sodium silicate phase Na_4SiO_4, and ZrO indicate the preference for sodium to attack the silica tetrahedra. The phases $Na_6Si_2O_7$ and $Na_2Si_2O_5$ indicate the possibility of a secondary reaction. The monomers, the sodium orthosilicate Na_4SiO_4, are polymerised to the dimers $Na_6Si_2O_7$ and possibly, ultimately to the sheets $Na_2Si_2O_5$. The metasilicate chains Na_2SiO_3 were not detected by the XRD, but could possibly be the intermediate between the dimers $Na_6Si_2O_7$ and sheets $Na_2Si_2O_5$. The phase $Na_2Si_2O_5$ was identified in traces, suggesting that the polymerisation at this stage is not the dominant reaction.

The new infrared band at 686 cm^{-1} (Fig. 8.3-8.5) is an indication of the δ(Si-O-Si) bending vibrations in a polymerised silicate structure e.g. $Na_2Si_2O_5$ or Na_2SiO_3 [7-9]. The XRD only revealed the phase $Na_2Si_2O_5$ at 650°C when fusing with six moles of sodium hydroxide. The presence of the infrared band at 686 cm^{-1}, between the frequency range 600-720 cm^{-1}, is taken as evidence of the presence of polymeric silicates [6-10]. This infrared band is seen for samples obtained at all the fusion temperatures. At 850°C the infrared band appears to be much broader. This could be an indication of the size of the silicate ring. The dependence of the position of this band on the number of ring members and the extent of its deformation has been determined: In the spectrum of glassy $Na_2Si_2O_5$ it has been shown that the infrared band is expected to be in the range of 740-600 cm^{-1} [9-10].

The infrared band at 864 cm^{-1} (Fig. 8.3-8.5) increases in intensity with increasing sodium hydroxide, but only for a fusion temperature of 650°C. This band can be assigned to the ν(Si-O^-) stretching vibrations of a non-bridging silico-oxygen found in a polymeric silicate [6-10].

When fusing a mole of zircon with six moles of sodium hydroxide at 650°C, the band is most intense. The XRD reveals traces of the phases $Na_6Si_2O_7$ and the silicate sheets $Na_2Si_2O_5$. The infrared band can be attributed to the ν(Si-O^-) stretching vibrations of a non-bridging silico-oxygen that is found in the XRD identified silicates [6-10].

The infrared stretching vibrations ν(Si-O-Si) at 900-960 cm^{-1} overlap with those due to zircon, but variations in intensity can be seen. These infrared bands were observed to increase in intensity with increments in sodium hydroxide (Fig 8.3-8.5). The bands indicate the development of Si-O-Si bridges [6-10].

The infrared spectra therefore suggest the presence of a polymerisation reaction. Under favourable conditions the orthosilicate monomers Na_4SiO_4, pyrosilicate dimers $Na_6Si_2O_7$ high in sodium and metasilicate chains Na_2SiO_3 can be polymerised to the disilicate sheets $Na_2Si_2O_5$ (scheme 8.1). The polymerisation reaction is *pseudo*-catalysed by the sodium, because it is first consumed to form the monomer and subsequently released as the oxide Na_2O to further decompose the zircon lattice.

$$2\ Na_4SiO_4 \longrightarrow Na_6Si_2O_7 + Na_2O \qquad (8.1A)$$

$$Na_6Si_2O_7 \longrightarrow 2Na_2SiO_3 + Na_2O \qquad (8.2B)$$

$$2Na_2SiO_3 \longrightarrow Na_2Si_2O_5 + Na_2O \qquad (8.3C)$$

SCHEME 8.1: A reaction scheme on the possible polymerisation reactions of the silicates during the prolonged decomposition of zircon at 650°C.

The presence, and the increasing intensity of the infrared band ν(Si-O^-) at 864 cm^{-1} with increase in NaOH, shows the preference for sodium to form sodium silicates (high in sodium) at 650°C rather than to attack the edge cell connected bisdisphenoids to form sodium zirconates. This suggests that the high stability of zircon is mainly due to the ZrO_8 bisdisphenoids edge cell connections.

The infrared band at 864 cm^{-1} was observed to decrease in intensity as the temperature was increased (Fig. 8.4-8.5); for instance at 850°C fusion with six moles of sodium hydroxide, the intensity of this band was negligible. This suggests that at high temperatures the sodium was not selective in its decomposition of the zircon lattice but attacked both SiO_4 silica tetrahedra and ZrO_8 bisdisphenoid linkages. This is corroborated by the phases identified in the XRD: sodium metasilicate, sodium zirconates and zircon (Figure 8.7-8.14).

8.3.2 ZIRCON DECOMPOSITION AFTER 336 HOURS OF FUSION

In order to determine the thermodynamically stable phases at the different reagent ratios, fusions were carried out for 336 hours with intermediate milling after every twenty-four hours. Fusion of a mole of zircon with one mole of sodium hydroxide was also considered.

Figures 8.15 to 8.18 show the infrared spectra obtained from the fusion products obtained after two weeks of fusion with periodic milling. The infrared stretching vibrations ν(Si-O-Si) at 900-960cm^{-1} and the bending vibrations δ(Si-O-Si) at 550-800 cm^{-1} (associated with rings/polymeric silicates) [6-10] are much more distinct at this stage and cannot be confused with that of zircon anymore.

The infrared bands at 742, 710 and 600cm^{-1} support the presence of silicate rings. The infrared band at 742cm^{-1} can also be attributed to monoclinic zirconia as seen in the raw spectra (Figure 8.38). The bands are now much broader that previously (at two hours of fusion). The 710 cm^{-1} band position corresponds to three membered rings. The infrared band at 600 cm^{-1}supports the presence of silicates with six membered rings. The band broadening supports the presence of silicate rings with more than six members.

Figure 8.23-24 shows the XRD pattern for the fusion of a mole of zircon with a mole of sodium hydroxide at 650°C for 336 hours. The phases ZrO_2 (trace), Na_2SiO_3 (trace) and $ZrSiO_4$ (major) were detected. Similar phases (and not their amounts) were detected when fusing a mole of zircon with two moles of sodium hydroxide (Figure 8.24). The zircon phase was detected in majority and the other phases in minority. The phases support the preference of sodium for the SiO_4 tetrahedra and the secondary reaction (Scheme 8.1). The secondary reaction is seen to progress only as far as the metasilicate chains.

The equilibrium phases (Scheme 8.2) were previously observed to form at much higher temperatures (~1480°C) [11-12]. The implied equilibrium reaction at 650°C and low $NaOH/ZrSiO_4$ mole ratios is:

$$ZrSiO_4 + Na_2O \longrightarrow ZrO_2 + Na_2SiO_3$$

SCHEME 8.2: The equilibrium reaction between zircon and sodium hydroxide at 850°C for $NaOH/ZrSiO_4 \leq 2$ mole ratio.

Figure 8.25 shows the XRD pattern for the fusion of a mole of zircon with four moles of sodium hydroxide at 650°C for 336 hours. The phases Na_2ZrO_3 (major), Na_2SiO_3 (major), Na_4SiO_4 (trace), ZrO_2 (trace) and $ZrSiO_4$ (minor) were observed. The presence of phases Na_4SiO_4 (trace), ZrO_2 (trace) suggest that the reaction was not yet at equilibrium. The presence and quantity of Na_2SiO_3 (major) supports the secondary reaction as seen in Scheme 8.1. The reaction is seen to only progress as far as the metasilicate chains. The presence and quantity of Na_2ZrO_3 suggests that the amount of sodium hydroxide is another thermodynamic parameter that governs the stability of the zircon structure. The quantity of the XRD phases suggests that reaction in Scheme 8.3 is predominant. Under favourable conditions the equilibrium reaction is:

$$ZrSiO_4 + 2Na_2O \longrightarrow Na_2ZrO_3 + Na_2SiO_3$$

SCHEME 8.3: The equilibrium reaction between sodium hydroxide and zircon at 650°C for $NaOH/ZrSiO_4 \geq 4$ mole ratio.

Figure 8.26 shows the XRD pattern for the fusion of a mole of zircon with six moles of sodium hydroxide at 650°C for 336 hours. The phases Na_2ZrO_3 (major), Na_2SiO_3 (major), Na_4SiO_4 (minor), ZrO_2 (minor) and $ZrSiO_4$ (minor) were observed. The presence of phases Na_4SiO_4 and ZrO_2 are seen to increase in amount when compared with those at four moles of NaOH. This suggests that equilibrium was not attained.

The presence of zircon suggests that this cannot be a point of complete decomposition. This can be attributed to the Na_4SiO_4 orthosilicate monomers that consume high amounts of sodium when decomposing the zircon lattice and the extent of polymerisation.

Figures 8.27 shows the XRD pattern for the fusion of a mole of zircon with one mole of sodium hydroxide at 850°C for 336 hours (intermediate milling). The phases $Na_4Zr_2Si_3O_{12}$ (major), Na_2ZrSiO_5 (minor), ZrO_2 (major) and $ZrSiO_4$ (major) were detected.

The phase $Na_4Zr_2Si_3O_{12}$ was reported to form after prolonged fusion [11]. It is a consequence of the reaction between Na_2ZrSiO_5 and Na_2SiO_3 with the liberation of Na_4SiO_4 (Scheme 8.4 reaction 8.4C). The orthosilicate Na_4SiO_4 when liberated should undergo the reaction in scheme 8.1 only as far as the metasilicate. The quantity of the phase $Na_4Zr_2Si_3O_{12}$ suggests that the reaction 8.4B in Scheme 8.4 predominates under these conditions.

Figures 8.28 shows the XRD pattern for the fusion of a mole of zircon with two moles of sodium hydroxide at 850°C for 336 hours (intermediate milling), the phases $Na_4Zr_2Si_3O_{12}$ (trace), Na_2ZrSiO_5 (major), ZrO_2 (trace) and $ZrSiO_4$ (trace) were identified. The amount of Na_2ZrSiO_5 is seen to increase and that of $Na_4Zr_2Si_3O_{12}$ and ZrO_2 decrease. The reactions suggested under favourable conditions are:

$$ZrSiO_4 + Na_2O \longrightarrow Na_2ZrSiO_5 \qquad (8.4A)$$

$$3ZrSiO_4 + 2Na_2O \longrightarrow Na_4Zr_2Si_3O_{12} + ZrO_2 \qquad (8.4B)$$

$$2Na_2ZrSiO_5 + 2Na_2SiO_3 \longrightarrow Na_4Zr_2Si_3O_{12} + Na_4SiO_4 \qquad (8.4C)$$

SCHEME 8.4: The equilibrium reaction between zircon and sodium hydroxide at 850°C for $NaOH/ZrSiO_4 \leq 2$ mole ratio. Reaction 8.4A predominates when fusing a mole of zircon with two moles of NaOH. The reaction 8.4B predominates at amounts less than two moles of fusion (e.g. one mole of NaOH per mole of zircon).

Figure 8.29 shows the XRD pattern for the fusion of a mole of zircon with four moles of sodium hydroxide at 850°C for 336 hours. The phases Na_2ZrO_3 (major), Na_2SiO_3 (minor), Na_2ZrSiO_5 (major) were detected. The quantity of Na_2ZrSiO_5 suggests that reaction 8.5A in Scheme 8.5 predominates. The phases were detected at much higher temperatures but at comparable amounts of sodium hydroxide. No zircon phase was detected, suggesting that this is possibly a point of complete decomposition. The infrared (Figure 8.18) further supports this point by the absence of the zircon characteristic band at 614 cm^{-1}.

The phase Na_2ZrSiO_5 was identified in majority, suggesting that the improved zircon decomposition is due to this phase.

Unlike the Na_4SiO_4 orthosilicates, this phase consumes low amounts of sodium (two moles less) while liberating a mole of zirconia form the zircon lattice.

Under favourable conditions the following reactions are possible:

$$ZrSiO_4 + Na_2O \longrightarrow Na_2ZrSiO_5 \qquad (8.5A)$$

$$ZrSiO_4 + 2Na_2O \longrightarrow Na_2ZrO_3 + Na_2SiO_3 \qquad (8.5B)$$

SCHEME 8.5: The reaction between zircon and sodium hydroxide at 850°C for $NaOH/ZrSiO_4 \geq 4$ mole ratio. Reaction 8.4A and 8.4B predominate when fusing a mole of zircon with four moles of NaOH. Reaction 8.5B predominates when fusing a mole of zircon with six moles of NaOH.

Figure 8.30 shows the XRD pattern for the fusion of a mole of zircon with six moles of sodium hydroxide at 850°C for 336 hours. The phases Na_2ZrO_3 (major), Na_2SiO_3 (minor) and ZrO_2 (trace) were detected. The quantity of Na_2ZrO_3 phase suggests that reaction 8.5B in Scheme 8.5 predominates. No zircon phase was detected, suggesting that this is possibly a point of complete decomposition. The infrared (Figure 8.18) further supports this point by the absence of the zircon characteristic band at 614 cm^{-1}.

Figures 8.19 to 8.22 show the Raman spectra obtained from the fusion products after 336 hours of fusion and periodic milling. Raman bands due to zircon (353, 435, 996, 1002, 1054 and 1458 cm^{-1}) dominate the Raman spectra at 650°C. This is further evidence (together with the XRD and IR) of the incomplete decomposition in this temperature region.

The Raman spectrum (Fig. 8.21) when fusing at 850°C with four or six moles of sodium hydroxide shows no bands due to zircon. The XRD and IR further support this observation. Raman bands at 400 to 510 cm^{-1} can be attributed to inter tetrahedral linkages Si-O-Si. The shift towards lower wavenumbers can be attributed to the heavy Zr^{4+} ion especially in the XRD identified phase $Na_4Zr_2Si_3O_{12}$ [14].

The Raman bands at 850 cm^{-1}, characteristic of the orthosilicate monomers, those at 900cm^{-1} for the pyrosilicate dimers, the 1000-950 cm^{-1} band of the metasilicate chains and the 1100-1050cm^{-1} band due to disilicate sheets were all not observed.

Griffith (1969) [13] suggests that the Raman bands due to the groups (SiO_n) are very weak owing to the small degree of π-bonding in the Si-O linkages. A mathematical deconvolution (to resolve a spectrum into its constituent bands) of the Raman spectra could be more descriptive as to the presence or absence of these bands. Thus their absence could be attributed to their low intensities [13-14].

8.4 EXPERIMENTAL DETERMINATION (MASS BALANCE APPROACH)

8.4.1 SODIUM DETERMINATION

The possibility of the reactions suggested by the XRD, IR and Raman were checked experimentally. The amount of sodium in the in-situ zirconates and silicates was determined with the aid of titration with standardised HCl. Experimental procedure described in Section 7.4.3 were employed. The yields of zirconia, silica and unreacted zircon were determined. A mass balance for reactions was done for two hour fusion time with no intermediate milling step is provided (Appendix A-F). Appendix G provides a mass balance of yields obtained after 336 hours of fusion and intermediate milling. Theoretically calculated values of the expected zirconia and silica yields are provided in Appendix H; theoretically expected amounts of sodium are provided in Appendix I.

8.4.2 SODIUM RECOVERY AT 650°C

Determination of the sodium (Figure 8.43, Appendix F) after 336 hours at 650°C when fusing with $NaOH/ZrSiO_4 \leq 2$ mole ratio, showed that most of the sodium (~99% Na_2O m/m) was dissolved with the silicates. This suggests that the zirconium compound in the AFDZ was low in sodium or hydrolysed easily.

The results are consistent with:

- sodium zirconate releasing half its sodium when hydrolysed in the water wash, and
- The sodium silicates being completely soluble in water.

Thus the expected NaOH recovery should be 100, 75 and 66,7% for $NaOH/ZrSiO_4$ mole ratios of 2, 4 and 6 respectively. In actual fact the values observed were 99, 69 and 65%.

When fusing for 2 hours at 650°C with a $NaOH/ZrSiO_4 \leq 4$ mole ratio most of the sodium (~79% Na_2O m/m) was recovered with the silicates (Figure 8.42, Appendix B). Besides the formation of the phases Na_2SiO_3 or Na_4SiO_4 and the hydrolysis of zirconates, the increased sodium content could be due to unreacted Na_2O. The NaOH recovery increases to a value of approximately 85.0 % Na_2O m/m in the soluble solids when fusing with $NaOH/ZrSiO_4 = 6$ mole ratio; this effect is attributed is also attributed to the unreacted Na_2O.

8.4.3 SODIUM RECOVERY AT 850°C

When fusing with $NaOH/ZrSiO_4 \leq 2$ mole ratio at 850°C for 336 hours most of the sodium (~99% Na_2O m/m) was retained as insoluble zirconates or sodium zirconium silicates (Figure 8.43, Appendix J). This implies that soluble sodium silicates were not formed. When the reagent mole ratio is increased to $NaOH/ZrSiO_4 = 4$ the sodium recovery increases to 65.0 %. This is attributed to the formation of Na_2SiO_3, Na_4SiO_4 and Na_2ZrO_3. Thus the increase can be attributed to the solubility of the sodium silicates and the partial hydrolysis of the zirconates to hydrous zirconia.

The determination of sodium to predict what phases have formed remains an inaccurate approach. This method is limited by the hydrolysis of the zirconates or sodium zirconium silicates and unreacted sodium hydroxide, but the method is useful in indicating the sodium content of the by-product.

8.5 THE SODIUM SILICATE BY-PRODUCT

Figure 8.33 shows the SEM photograph of the alkali silicate by-product. The by-product was tacky and adhered strongly to the borosilicate glass beakers. Figure 8.36 shows the infrared spectrum of the alkali silicate. Bands due to sodium metasilicate dominate the spectrum but bands due to sodium carbonate at 1 448 and 1 411cm^{-1} were also observed [6]. Figure 8.46 shows the X-ray diffraction pattern of the alkali silicate the presents of the carbonate is further supported. The elemental analysis is given in Appendix K. The by-product was very high in sodium when compared to the metasilicate Na_2SiO_3.

8.6 ZIRCONIUM SULPHATE TETRAHYDRATE

Figure 8.34 shows the SEM photograph of AZST obtained by water evaporation of an aqueous solution of the normal sulphate salt. Large crystalline particles with no particular morphology can be seen. Figure 8.37 shows the infrared spectrum of AZST.

The spectrum shows bands predominantly due to the AZST molecular vibrations [4, 6]. Figure 8.47 shows the X-ray diffraction pattern of AZST. Many phases of the salt $Zr(SO_4)_2.5H_2O$ were identified [5]. This can be attributed to the complex crystallisation of the normal sulphate and conditions at room temperature, which encourage the crystallisation of the pentahydrate. The elemental analysis is given in Appendix K. The product is of very high purity.

8.7 ZIRCONIA

Figure 8.35 shows the SEM photographs of zirconia. Regular, but agglomerated, oblong particles are visible. Figure 8.38 and 8.39 show the infrared and Raman spectra of zirconia; bands due to monoclinic zirconia dominate the spectra. The strong absorption band that was confused with the zirconyl group at 1 100cm^{-1} can be clearly seen [4]. The band at 748 cm^{-1} can be attributed to Zr-O-Zr vibrations. Figure 8.48 shows the X-ray diffraction pattern of zirconia.

The intensity of the spectrum suggests the predominance of monoclinic zirconia and that tetragonal zirconia formed in trace amounts. The elemental analysis is given in Appendix K. The product purity exceeds 98,4% ZrO_2 with HfO_2 > 1,1%.

8.8 CONCLUSIONS

The decomposition of zircon was carried out in open reaction vessels. A mole of zircon was decomposed using from one to six moles of sodium hydroxide and fusion temperatures of 650, 750 and 850°C. When the fusion time is limited to two hours non-equilibrium phases form and the products formed depend on reaction kinetics. For prolonged fusion times (e.g. 336 hours) the reaction products tend towards the expected equilibrium phases. These are the two factors that determine phase formation.

The tetragonal structure of zircon is stabilised by the bisdisphenoids linkages. The silicate phases that are formed can be polymerised to silicates low in sodium (e.g. Na_2SiO_3 or $Na_2Si_2O_5$). This allows the sodium to be released for further decomposition reactions. At 850°C and long fusion times the phases observed are thermodynamically stable one to those reported for higher temperatures by D'Ans and Loeffler (1930) [11]. However, the phase diagram observed at 650°C differs from that obtained by them: The phases Na_2ZrSiO_5 and $Na_4Zr_2Si_3O_{12}$ were not observed.

8.8.1 DECOMPOSITION AT 650°C

Prolonged fusion at 650°C with $NaOH/ZrSiO_4 \leq 2$ mole ratio leads to the formation of sodium metasilicate and zirconia (Scheme 8.2). The XRD reveals the presence of metasilicate and zirconia in trace- or in minor amounts. The low level of detection of these compounds could be due to an amorphous state of the samples (Figure 8.24). The IR bands at 710 and 600 cm^{-1}, support the presence of polymerised silicates (e.g. the sodium metasilicate).

Prolonged fusion (336 hours) at 650°C with $4 \leq NaOH$ moles ≤ 6 leads to the formation of sodium silicates high in sodium and the polymerisation (Scheme 8.1) of the orthosilicate monomers to metasilicate chains. The IR supports this conclusion showing the presence of the δ(Si-O-Si) band at 686 cm^{-1} (for the fusion done in two hours). The split in the band at 686 to ones at 710 and 600 cm^{-1} is indicative of the presence of highly polymerised silicates. The band at 600 cm^{-1}indicates the presents of silicates with rings with more than six members [6-10].

When fusing for two hours, increasing the amount of sodium hydroxide leads to the formation of silicates high in sodium (e.g. Na_4SiO_4) and zirconia. Zirconia, in its reduced state, is formed rather than sodium zirconate. This is a consequence of the stability of the ZrO_8 bisdisphenoids and the instability of the SiO_4 tetrahedra linkages at this temperature.

For prolonged fusion with $NaOH/ZrSiO_4 \leq 2$ mole ratio, most of the sodium followed the silicates. This suggests that the zirconium compound in the AFDZ was low in sodium or hydrolysed easily.

8.8.2 DECOMPOSITION AT 850°C

When zircon is decomposed with sodium hydroxide at higher temperatures e.g. 850°C, the formation of sodium silicates and sodium zirconates is observed. This is an indication that at this temperature the ZrO_8 bisphenoid linkages are not resistant to Na_2O attack.

Prolonged fusion (e.g. 336 hours) at 850°C with $NaOH/ZrSiO_4 < 2$ mole ratio leads to the formation of the phase $Na_4Zr_2Si_3O_{12}$ and ZrO_2 (Scheme 8.4). Prolonged fusion at 850°C with $NaOH/ZrSiO_4 = 2$ mole ratio leads to the formation of the phase Na_2ZrSiO_5 (Scheme 8.4). The formation of these phases ($Na_4Zr_2Si_3O_{12}$ and Na_2ZrSiO_5) was not detected at 650°C.

8.8.3THE PRODUCTS

The by-product contains sodium metasilicate as well as sodium carbonate. The presence of the latter is attributed to the reaction of atmospheric carbon dioxide with excess sodium during crystallisation. The observed Na_2O/SiO_2 mol ratio, in the sodium silicate stream, exceeded three for all reagent ratios for a 2 hour fusion time.

The zirconium sulphate tetrahydrate (AZST) prepared in this study consists of many phases owing to the nature of the crystallisation process. Similar observations were made by Bear and Mumme (1971) [6]. Appendix K confirms that a product of very high purity can be obtained.

The zirconia prepared in this study is predominantly monoclinic. It consisted of oblong, spherical particles with a dimension of about 90 nm. The zirconia obtained was also of high purity as shown in Appendix K.

8.9 REFERENCES

1. Nielsen, R. Chang, T. W. (1996) Ullman's Encyclopaedia of Industrial Chemistry, A (28) 543-567.
2. Hancock, J. D. (1977) A review of conventional and novel processes for the extraction of zirconia from zircon. Mineral Science and Engineering, (9) 25-31.
3. Houchin, M. R. Jenkins, B. E. Sinha, H. N. (1990) Production of high quality zirconia for ceramics, Mineral, Materials and Industry 14th congress of the council of mining and metallurgy Institute, organised by IMM.
4. Clearfield, A. (1964) Structural aspects of Zirconium Chemistry. Rev. Pure and Appl. Chem. (14) 9
5. Bear, I. J. and. Mumme, W. G. (1971) Normal Sulphates of Zirconium and Hafnium, Rev. Pure and Appl. Chem., (21) 189.
6. Nakamoto, K. (1986) The infrared and Raman spectroscopy of inorganic and coordination compounds, 4th edition. A John Wiley and Sons publication, New York.
7. Sitarz, M. Mozgawa, W. Handke, M. (1999) Rings in the structure of silicate glasses, Journal of Molecular Structure, (511-512) 281-285.
8. Mysen, B. O. Virgo, D. Seifert, F. A. (1982) Am. Min. (67) 686-695.
9. Sitarz, M. Moozgawa, W. Handke, M. (1997) Vibrational spectra of complex ring silicate anions-method of recognition, Journal of Molecular structure, (404), 193-197.
10. Huang, Y. Zhimei, J. and Schwieger, W. (1999) Vibrational spectroscopic studies of layered silicates, Chem. Mater. (11), 1210-1217.
11. D' Ans, J. and Loeffler, J. (1930) Z. Anorg. Allg. Chem., (191) [1-2], 22.
12. Sircar, A. and Brett, N. H. (1970) Trans. Brit. Ceram. Soc., (69) [3], 133.
13. Macmillan, P. (1984) Structural studies of silicate glasses and melts-application and limitations of Raman spectroscopy, Am. Min, (69) 622-644.
14. Griffith, W. P. (1969) Raman Studies on rock-forming minerals. Part 1. Orthosilicates and Cyclosilicates, J. Chem. Soc. (A), 1372-1377.
15. Furukawa, T. Fox, E. K. White, W. B. (1981) Raman spectroscopic investigation of silicate glasses. III. Raman intensities and structural units in sodium silicate glasses, J. Chem. Phys., (75) No 7, 3227-3237.
16. Atkins, P.W. (1990) Physical chemistry, Oxford Univ. press, Oxford.